
Extrinsic Methods for Coding and Dictionary Learning on Grassmann Manifolds

Mehrtash Harandi · Richard Hartley ·
Chunhua Shen · Brian Lovell ·
Conrad Sanderson

Feb. 2014

Abstract Sparsity-based representations have recently led to notable results in various visual recognition tasks. In a separate line of research, Riemannian manifolds have been shown useful for dealing with features and models that do not lie in Euclidean spaces. With the aim of building a bridge between the two realms, we address the problem of sparse coding and dictionary learning over the space of linear subspaces, which form Riemannian structures known as Grassmann manifolds. To this end, we propose to embed Grassmann manifolds into the space of symmetric matrices by an isometric mapping. This in turn enables us to extend two sparse coding schemes to Grassmann manifolds. Furthermore, we propose closed-form solutions for learning a Grassmann dictionary, atom by atom. Lastly, to handle non-linearity in data, we extend the proposed Grassmann sparse coding and dictionary learning algorithms through embedding into Hilbert spaces.

Experiments on several classification tasks (gender recognition, gesture classification, scene analysis, face recognition, action recognition and dynamic texture classification) show that the proposed approaches achieve considerable improvements in discrimination accuracy, in comparison to state-of-the-art methods such as kernelized Affine Hull Method and graph-embedding Grassmann discriminant analysis.

M. Harandi and R. Hartley
College of Engineering and Computer Science, Australian National University, and
NICTA, Australia
E-mail: mehrtash.harandi@nicta.com.au
E-mail: richard.hartley@nicta.com.au

C. Shen
School of Computer Science, The University of Adelaide, SA 5005, Australia
E-mail: chunhua.shen@adelaide.edu.au

B. Lovell
The University of Queensland, St Lucia, Australia
E-mail: lovell@itee.edu.au

C. Sanderson
Queensland University of Technology, and NICTA, Australia
E-mail: conrad.sanderson@nicta.com.au

Keywords Riemannian geometry · Grassmann manifolds · sparse coding · dictionary learning

1 Introduction

This paper introduces techniques to represent p -dimensional linear subspaces in \mathbb{R}^n using a combination of linear subspaces. Linear subspaces can be considered as the core of many inference algorithms in computer vision and machine learning. For example, several state-of-the-art methods for matching videos or image sets model given data by subspaces (Hamm and Lee 2008; Harandi et al. 2011; Turaga et al. 2011; Vemulapalli et al. 2013; Sanderson et al. 2012; Chen et al. 2013). Auto regressive and moving average models, which are typically employed to model dynamics in spatio-temporal processing, can also be expressed as linear subspaces (Turaga et al. 2011). More applications of linear subspaces in computer vision include, but are not limited to, chromatic noise filtering (Subbarao and Meer 2009), and domain adaptation (Gong et al. 2012; Gopalan et al. 2013).

Despite their wide applications and appealing properties (*e.g.*, the set of all reflectance functions produced by Lambertian objects lies in a linear subspace), subspaces lie on a special type of Riemannian manifold, namely the Grassmann manifold, which makes their analysis very challenging. This paper tackles and provides efficient solutions to the following two fundamental problems for learning on Grassmann manifolds:

1. **Coding.** Given a subspace \mathbf{X} and a set $\mathbb{D} = \{\mathbf{D}_i\}_{i=1}^N$ with N elements (also known as atoms), where \mathbf{X} and \mathbf{D}_i are linear subspaces, how can \mathbf{X} be approximated by a combination of atoms in \mathbb{D} ?
2. **Dictionary learning.** Given a set of measurements $\{\mathbf{X}_i\}_{i=1}^m$, how can a set $\mathbb{D} = \{\mathbf{D}_i\}_{i=1}^N$ be learned to represent $\{\mathbf{X}_i\}_{i=1}^m$ accurately?

Our main motivation here is to develop new methods for analyzing video data and image sets. This is inspired by the success of sparse signal modeling and related topics that suggests natural signals like images (and hence video and image sets as our concern here) can be efficiently approximated by superposition of atoms of a dictionary. We generalize the traditional notion of coding, which operates on vectors, to sparse coding on subspaces. Sparse encoding with the dictionary of subspaces can then be seamlessly used for categorizing video data.

1.1 Prior Work

In the past decade, sparsity has become a popular term in neuroscience, information theory, signal processing and related areas (Elad 2010; Candes et al. 2006; Olshausen and Field 1996; Wright et al. 2009). Through sparse representation and compressive sensing it is possible to represent natural signals like images using only a few non-zero coefficients of a suitable basis (Elad 2010). In the computer vision community, sparse and overcomplete image models were first introduced for modeling the spatial receptive fields of simple cells in the human visual system by Olshausen and Field (1996). The linear decomposition of a signal using a few atoms of a dictionary has been shown to deliver notable results for various

visual inference tasks, such as face recognition (Wright et al. 2009) and image classification (Yang et al. 2009). While significant steps have been taken to develop the theory of the sparse coding and dictionary learning in Euclidean spaces, similar problems on non-Euclidean geometry have received comparatively little attention (Harandi et al. 2012; 2013a; Ho et al. 2013). To our best knowledge, except the preliminary version of this paper (Harandi et al. 2013a), among a handful of solutions devised on Riemannian manifolds, none is specialized for Grassmann manifolds.

Inference on manifold spaces can be achieved extrinsically by embedding the manifolds in Euclidean spaces (possibly higher dimensional), which can be considered as flattening the manifolds. In the literature, the most popular choice for embedding manifolds is through considering tangent spaces (Tuzel et al. 2008; Subbarao and Meer 2009; Faraki et al. 2013). For example, Tuzel et al. (2008) tackled the problem of pedestrian detection through a classifier that utilized several tangent spaces. Subbarao and Meer (2009) reformulated the mean shift algorithm (Comaniciu and Meer 2002) over non-linear manifolds, where the mean shift can be seen as an iterative approach that switches between manifold and tangent spaces.

Flattening manifolds through tangent spaces is not free of drawbacks, as only distances between points to the tangent pole are equal to true geodesic distances. This is restrictive and may lead to inaccurate modeling. An alternate methodology considers embedding manifolds into Reproducing Kernel Hilbert Spaces (RKHS) (Hamm and Lee 2008; Harandi et al. 2012; Jayasumana et al. 2013; Harandi et al. 2013b). This in turn opens the door for employing many kernel-based machine learning algorithms (Shawe-Taylor and Cristianini 2004). For example, in (Harandi et al. 2012), we addressed sparse coding and dictionary learning for the Riemannian structure of symmetric positive definite matrices or tensors by using a Riemannian kernel.

Focusing on the problem of coding and dictionary learning on Grassmann manifolds, Ho et al. (2013) recently proposed a general framework to learning a Riemannian dictionary by exploiting tangent bundles of the manifold. Since sparse coding has a trivial solution in this approach, an affine constraint has to be added to the problem (Ho et al. 2013). While having an affine constraint along with sparse coding is welcome in specific tasks (*e.g.*, clustering (Cetingul and Vidal 2009)), in general, the resulting formulation is restrictive and no longer addresses the original problem. Furthermore, working in successive tangent spaces, though common, values only a first-order approximation to the manifold at each step. Lastly, switching back and forth to the tangent spaces of a Grassmann manifold (as required by this formulation) can be computationally very demanding for the problems that we are interested in (*e.g.*, video analysis). This in turns makes the applicability of such school of thought too limited for the Grassmann manifolds arising in vision tasks.

Contributions. In light of the above discussion, in this paper we introduce an extrinsic method for learning a Grassmann dictionary. To this end, we propose to embed Grassmann manifolds into the space of symmetric matrices by a diffeomorphism that preserves Grassmann projection distance (a special class of distances on Grassmann manifolds). We show how sparse coding can be accomplished in the induced space and devise a closed-form solution for updating a Grassmann dictionary atom by atom. Furthermore, in order to accommodate non-linearity in data,

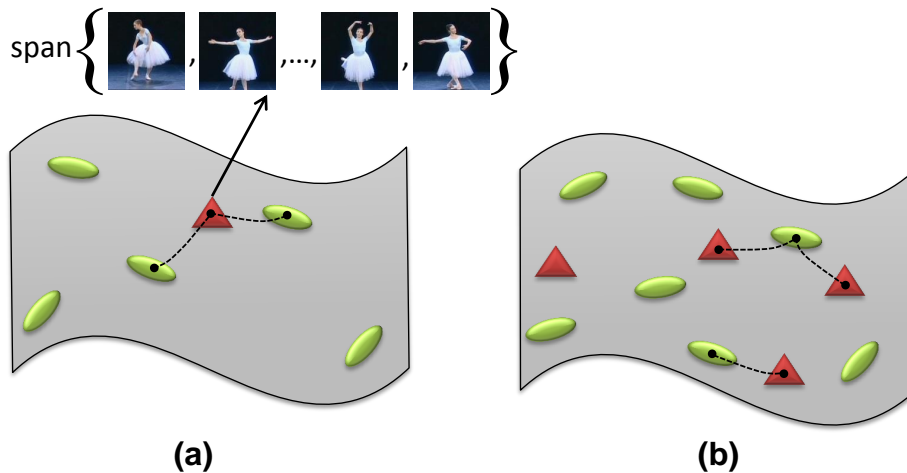


Fig. 1: A conceptual diagram of the problems addressed in this work. A video or an image set can be modeled by a linear subspace, which can be represented as a point on a Grassmann manifold. **(a) Sparse coding on a Grassmann manifold.** Given a dictionary (green ellipses) and a query signal (red triangle) on the Grassmann manifold, we are interested in estimating the query signal by a sparse combination of atoms while taking into account the geometry of the manifold (*e.g.*, curvature). **(b) Dictionary learning on a Grassmann manifold.** Given a set of observations (green ellipses) on a Grassmann manifold, we are interested in determining a dictionary (red triangles) to describe the observations sparsely, while taking into account the geometry. This figure is best seen in color.

we propose kernelized versions of our coding and dictionary learning algorithms. Our contributions are therefore three-fold:

1. We propose to perform coding and dictionary learning for data points on Grassmann manifolds by embedding the manifolds into the space of symmetric matrices¹.
2. We derive kernelized versions of the proposed coding and dictionary learning algorithms (*i.e.*, embedded into Hilbert spaces), which can address non-linearity in data.
3. We apply the proposed Grassmann dictionary learning methods to several computer vision tasks where the data are videos or image sets. Our proposed algorithms outperform state-of-the-art methods on a wide range of classification tasks, including gender recognition from gait, scene analysis, face recognition from image sets, action recognition and dynamic texture classification.

¹ The embedding we consider in this work results in symmetric but rank-deficient matrices. As such, methods devised to exploit the Riemannian structure of symmetric positive definite matrices, such as (Harandi *et al.* 2012), cannot be employed here.

2 Background Theory

This section overviews Grassmann geometry and provides the groundwork for techniques described in following sections. We first describe the notion of manifolds and their properties including tangent spaces and geodesics. Since the term “manifold” itself is often used in computer vision in a somewhat loose sense, we emphasize that the word is used in this paper in its strict mathematical sense.

Throughout the paper, bold capital letters denote matrices (*e.g.* \mathbf{X}) and bold lower-case letters denote column vectors (*e.g.* \mathbf{x}). The notations $[\cdot]_i$ and $[\cdot]_{i,j}$ are used to demonstrate elements in position i and (i, j) in a vector and matrix, respectively. $\mathbf{1}_d \in \mathbb{R}^d$ and $\mathbf{0}_d \in \mathbb{R}^d$ are vectors of ones and zeros. \mathbf{I}_d is the $d \times d$ identity matrix. $\|\mathbf{x}\|_1 = \sum_i |[x]_i|$ and $\|\mathbf{x}\| = \sqrt{\mathbf{x}^T \mathbf{x}}$ denote the ℓ_1 and ℓ_2 norms, respectively, with T showing transposition. $\|\mathbf{X}\|_F = \sqrt{\text{Tr}(\mathbf{X}^T \mathbf{X})}$ designates the Frobenius norm, with $\text{Tr}(\cdot)$ computing the matrix trace.

2.1 Manifolds, Geodesics and Tangent Spaces

Intuitively, we can think of manifolds as extension of curves and surfaces to higher dimensional spaces, albeit with the property of being locally Euclidean. That is, Euclidean geometry such as parallel postulate is only valid for a neighborhood around each point. For example, the unit sphere is a two dimensional manifold lying in 3D Euclidean space. Below we provide formal definitions of manifolds.

Definition 1 (Topological Manifold) An n -dimensional, second countable, Hausdorff space \mathcal{M} is called a manifold if it is locally homeomorphic to Euclidean space, *i.e.*, for every point $\mathbf{x} \in \mathcal{M}$ there exists a neighborhood $\mathcal{U} \subset \mathcal{M}$ containing \mathbf{x} and an associated mapping φ from \mathcal{U} to an Euclidean space \mathbb{R}^d , such that $\varphi(\mathcal{U})$ is an open set \mathbb{R}^d (Lee 2012).

Besides being locally Euclidean which is reflected through the homeomorphic property, the space needs to be second countable and Hausdorff. The property of being second countable ensures that the space has a countable base (intuitively, the manifold can be covered by a countable set of local Euclidean patches). In a Hausdorff space, distinct points have disjoint neighborhoods. This property is useful for establishing the notion of a differential manifold, as Hausdorffness is practically the most common way of ensuring that convergent sequences have a single limit point. The neighborhood \mathcal{U} and its associated mapping φ together form a coordinate chart (\mathcal{U}, φ) .

Definition 2 (Differentiable Manifold) A differentiable manifold is a smooth manifold, such that for all coordinate charts (\mathcal{U}, φ) and (\mathcal{V}, ψ) , either $\mathcal{U} \cap \mathcal{V} = \emptyset$ or if $\mathcal{U} \cap \mathcal{V}$ is non-empty then transition map $\varphi \circ \psi^{-1}$ is smooth, *i.e.*, it is infinitely differentiable.

The notion of differentiable manifold is required to perform calculus on manifolds. Attached to every point \mathbf{x} of a differentiable manifold \mathcal{M} , there exists a vector space that can be thought of as the set of allowed velocities by constraining the point \mathbf{x} to move on the manifold. The set of all such velocities or tangent vectors is called the tangent space to \mathcal{M} at \mathbf{x} and is denoted by $T_{\mathbf{x}}(\mathcal{M})$. Even

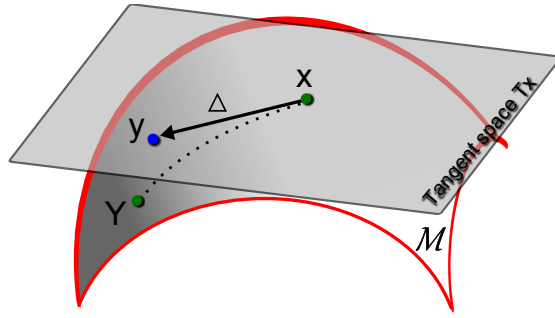


Fig. 2: Illustration of the tangent space $T_{\mathbf{X}}$ at point \mathbf{X} on a Riemannian manifold \mathcal{M} . The tangent vector Δ can be obtained through the logarithm mapping, *i.e.* $\Delta = \log_{\mathbf{X}}(\mathbf{Y})$. Every tangent vector in $T_{\mathbf{X}}$ can be mapped back to the manifold through the exponential map, *i.e.* $\exp_{\mathbf{x}}(\Delta) = \mathbf{Y}$. The dotted line shows the geodesic starting at \mathbf{X} and ending at \mathbf{Y} .

though the manifold \mathcal{M} may be nonlinear, the tangent space $T_{\mathbf{x}}(\mathcal{M})$ is always linear. Moreover, the dimensionality of $T_{\mathbf{x}}(\mathcal{M})$ is the same as of \mathcal{M} .

In many applications, the manifold of interest is Riemannian, which is a differentiable manifold endowed with a Riemannian metric, *i.e.*, an inner product defined on its tangent spaces. The Riemannian metric enables us to establish the notion of lengths and angles on the manifold. Two operators, namely the exponential map $\exp_{\mathbf{X}}(\cdot)$ and the logarithm map $\log_{\mathbf{X}}(\cdot) = \exp_{\mathbf{X}}^{-1}(\cdot)$, are defined over differentiable manifolds to switch between the manifold and tangent space at \mathbf{X} (see Fig. 2 for a conceptual illustration). The exponential operator maps a tangent vector Δ to a point \mathbf{Y} on the manifold. The logarithm map is the inverse of the exponential map and maps a point on the manifold to the tangent space $T_{\mathbf{X}}$. The exponential and logarithm maps vary as point \mathbf{X} moves along the manifold.

On a Riemannian manifold, points are connected via smooth curves. The distance between two points is defined as the length of shortest curve connecting them on the manifold. The shortest curve and its length are called geodesic and geodesic distance, respectively. For example, the geodesics on spheres are great circles.

The property of the exponential map ensures that the length of a tangent vector $\Delta = T_{\mathbf{X}}(\mathbf{Y})$ is equivalent to the geodesic distance between \mathbf{X} and \mathbf{Y} . More involved treatments on manifolds and related topics are given by Absil *et al.* (2008) and Lee (2012).

2.2 Grassmann Manifold and its Riemannian structure

The space of $d \times p$, $0 < p < d$ matrices with orthonormal columns is not an Euclidean space but a Riemannian manifold known as Stiefel manifold $\mathcal{S}(p, d)$, *i.e.*,

$$\mathcal{S}(p, d) \triangleq \{\mathbf{X} \in \mathbb{R}^{d \times p} : \mathbf{X}^T \mathbf{X} = \mathbf{I}_p\}$$

By grouping together all points on $\mathcal{S}(p, d)$ that span the same subspace we obtain a Grassmann manifold $\mathcal{G}(p, d)$ (Absil *et al.* 2008). That is, the Grassmann manifold $\mathcal{G}(p, d)$ is the space of p -dimensional linear subspaces of \mathbb{R}^d for $0 < p < d$ (Absil *et al.* 2008). Formally,

Definition 3 (Grassmann Manifold) Grassmann manifold $\mathcal{G}(p, d)$ can be defined as a quotient manifold of $\mathcal{S}(p, d)$ with the equivalence relation \sim being: $\mathbf{X}_1 \sim \mathbf{X}_2$ if and only if $\text{Span}(\mathbf{X}_1) = \text{Span}(\mathbf{X}_2)$, where $\text{Span}(\mathbf{X})$ denotes the subspace spanned by columns of $\mathbf{X} \in \mathcal{S}(p, d)$, *i.e.*, two points are equivalent if they span the same subspace.

We note that in the special case $p = 1$, the Grassmann manifold becomes the projective space \mathbb{P}^{d-1} , which consists of all lines passing through the origin. A point on the Stiefel manifold $\mathcal{S}(p, d)$ is represented by an $d \times p$ matrix with orthonormal columns. A point on the Grassmann manifold $\mathcal{G}(p, d)$ is a linear subspace, which may be specified by an arbitrary orthogonal basis through an $d \times p$ matrix. Unlike points on Stiefel manifolds, the choice of matrix is not unique for points on Grassmann manifolds.

For Grassmann manifolds, tangent vectors at \mathbf{X} admit $\mathbf{X}^T \Delta + \Delta^T \mathbf{X} = 0$. This can be obtained by differentiating the orthogonality constraint $\mathbf{X}^T \mathbf{X} = \mathbf{I}_p$, $\forall \mathbf{X} \in \mathcal{G}(p, d)$. The Riemannian metric for two tangent vectors Δ_1 and Δ_2 at \mathbf{X} is defined as (Absil et al. 2008):

$$\langle \Delta_1, \Delta_2 \rangle_{\mathbf{X}} = \text{Tr} \left(\Delta_1^T \left(\mathbf{I}_p - \frac{1}{2} \mathbf{X} \mathbf{X}^T \right) \Delta_2 \right) = \text{Tr} \left(\Delta_1^T \Delta_2 \right).$$

This Riemannian metric induces a geodesic distance, $\delta_g(\cdot, \cdot)$ on the Grassmann manifold, namely the length of the shortest curve between two p -dimensional subspaces. The special orthogonal group $SO(d)$ (think of this as higher-dimensional rotations) acts transitively on $\mathcal{G}(p, d)$ by mapping one p -dimensional subspace to another. The geodesic distance may be thought of as the magnitude of the smallest rotation that takes one subspace to the other. If $\Theta = [\theta_1, \theta_2, \dots, \theta_p]$ is the sequence of principal angles (Absil et al. 2008) between two subspaces \mathbf{X}_1 and \mathbf{X}_2 , then

$$\delta_g(\mathbf{X}_1, \mathbf{X}_2) = \|\Theta\|_2. \quad (1)$$

Definition 4 (Principal Angles) Let \mathbf{X}_1 and \mathbf{X}_2 be two matrices of size $d \times p$ with orthonormal columns. The principal angles $0 \leq \theta_1 \leq \theta_2 \leq \dots \leq \theta_p \leq \pi/2$ between two subspaces $\text{Span}(\mathbf{X}_1)$ and $\text{Span}(\mathbf{X}_2)$, are defined recursively by

$$\begin{aligned} \cos(\theta_i) &= \max_{\mathbf{u}_i \in \text{Span}(\mathbf{X}_1)} \max_{\mathbf{v}_i \in \text{Span}(\mathbf{X}_2)} \mathbf{u}_i^T \mathbf{v}_i & (2) \\ \text{s.t.} & \quad \|\mathbf{u}_i\|_2 = \|\mathbf{v}_i\|_2 = 1 \\ & \quad \mathbf{u}_i^T \mathbf{u}_j = 0; \quad j = 1, 2, \dots, i-1 \\ & \quad \mathbf{v}_i^T \mathbf{v}_j = 0; \quad j = 1, 2, \dots, i-1 \end{aligned}$$

In other words, the first principal angle θ_1 is the smallest angle between all pairs of unit vectors in the first and the second subspaces. The rest of the principal angles are defined similarly. The cosines of principal angles are the singular values of $\mathbf{X}_1^T \mathbf{X}_2$ (Absil et al. 2008).

The exponential map and its inverse map do not have a closed-form solution for Grassmann manifolds. Efficient numerical approaches for computing both maps were proposed by Gallivan et al. (2003). For the sake of completeness, we provide the exponential and logarithm maps in Appendix B. Before concluding this section

we would like to mention that the Riemannian structure of linear subspaces was taken for granted here without providing any proof for that. One could prove that the set of p dimensional linear subspaces in \mathbb{R}^d form a differentiable manifold either through the notion of quotient space of orthogonal group $SO(d)$ or through the smooth manifold chart lemma (please see (Lee 2012) for details).

3 Problem Statement

We start this section by providing a general formulation for the problems of coding and dictionary learning in vector spaces. By *coding* we mean the general notion of representing a vector through other vectors. The notion of *sparse coding* is hence a specific case of coding. Given a query $\mathbf{x} \in \mathbb{R}^d$ and a dictionary \mathbb{D} of size N , *i.e.*, $\mathbb{D}_{d \times N} = [\mathbf{d}_1 | \mathbf{d}_2 | \dots | \mathbf{d}_N]$ with atoms $\mathbf{d}_i \in \mathbb{R}^d$, the problem of coding in vector spaces can be described by:

$$l_E(\mathbf{x}, \mathbb{D}) \triangleq \min_{\mathbf{y}} \left\| \mathbf{x} - \sum_{j=1}^N [\mathbf{y}]_j \mathbf{d}_j \right\|_2^2 + \lambda f(\mathbf{y}). \quad (3)$$

The idea here is to reconstruct (approximately) the query \mathbf{x} by a linear combination of dictionary atoms while enforcing the coefficients of combination, *i.e.*, \mathbf{y} , to have some structure. A good reconstruction is the one that has the minimum error which is reflected through the energy term $\|\cdot\|_2$ in Eq. (3). The structure of solution is enforced by the function $f: \mathbb{R}^N \rightarrow \mathbb{R}$ and could be for example sparsity as foreseen in sparse coding (Elad 2010) or some forms of locality as proposed by Wang et al. (2010).

The problem of dictionary learning is defined as determining \mathbb{D} given a finite set of observations $\mathbb{X} = \{\mathbf{x}_i\}_{i=1}^m$, $\mathbf{x} \in \mathbb{R}^d$, by optimizing the following objective function:

$$h(\mathbb{D}) \triangleq \sum_{i=1}^m l_E(\mathbf{x}_i, \mathbb{D}) \quad (4)$$

A “good” dictionary has a small reconstruction error over all observations \mathbb{X} while producing the codes $\mathbf{y}_i \in \mathbb{R}^N$ with the desired structure. For example, in the case of sparse coding, the ℓ_1 norm is usually employed as $f(\cdot)$ to obtain the most common form of dictionary learning in the literature. We note that with this choice, finding the optimum \mathbb{D} in Eq. (4) is still not trivial because of non-convexity, as can be seen by rewriting the dictionary learning to:

$$\min_{\{\mathbf{y}_i\}_{i=1}^m, \mathbb{D}} \sum_{i=1}^m \left\| \mathbf{x}_i - \sum_{j=1}^N [\mathbf{y}_i]_j \mathbf{d}_j \right\|_2^2 + \lambda \sum_{i=1}^m \|\mathbf{y}_i\|_1. \quad (5)$$

A common approach to solving this is to alternate between the two sets of variables, \mathbb{D} and $\mathbf{Y} = [\mathbf{y}_1 | \mathbf{y}_2 | \dots | \mathbf{y}_m]$, as proposed for example by Elad (2010). More specifically, minimizing Eq. (5) over sparse codes \mathbf{y}_i while dictionary \mathbb{D} is fixed is a convex problem. Similarly, minimizing the overall problem over \mathbb{D} with fixed $\{\mathbf{y}_i\}_{i=1}^m$ is convex as well.

Directly translating the coding (and consequently dictionary learning) problem to non-flat Grassmann manifolds results in re-casting Eq. (3) as:

$$l_G(\mathbf{X}, \mathbb{D}) \triangleq \min_{\mathbf{y}} \left\| \mathbf{X}_i \ominus \bigoplus_{j=1}^N [\mathbf{y}]_j \odot \mathbf{D}_j \right\|_{\mathcal{G}}^2 + \lambda f(\mathbf{y}). \quad (6)$$

Here $\mathbf{X} \in \mathbb{R}^{d \times p}$ and $\mathbf{D}_j \in \mathbb{R}^{d \times p}$ are points on Grassmann manifold $\mathcal{G}(p, d)$, while the operators \ominus and \uplus are Grassmann replacements for subtraction and summation in vector spaces (and hence should be commutative and associative). Furthermore, \odot is the replacement for scalar multiplication and $\|\cdot\|_{\mathcal{G}}$ is the geodesic distance on Grassmann manifolds.

There are several difficulties in solving Eq. (6). Firstly, \ominus , \uplus and \odot need to be appropriately defined. While the Euclidean space is closed under the subtraction and addition (and hence a sparse solution $\sum_{j=1}^N [\mathbf{y}]_j \mathbf{d}_j$ is a point in that space), Grassmann manifolds are not closed under normal matrix subtraction and addition. More importantly, Eq. (6) is not convex even for convex choices of $f(\cdot)$ because of the distance function $\|\cdot\|_{\mathcal{G}}$.

In this work, we propose to embed Grassmann manifolds into the space of symmetric matrices via the *projection embedding* $\Pi : \mathcal{G}(p, d) \rightarrow \text{Sym}(d)$, $\Pi(\mathbf{X}) = \mathbf{X}\mathbf{X}^T$. The projection embedding has been previously used in subspace tracking (Srivastava and Klassen 2004), clustering (Cetingul and Vidal 2009), discriminant analysis (Hamm and Lee 2008; Harandi et al. 2011) and classification purposes (Vemulapalli et al. 2013). A natural metric on $\text{Sym}(d)$ is induced by the Frobenius norm, $\|\cdot\|_F$ which we will exploit to *convexify* Eq. (6). As such, we define:

$$\delta_s(\mathbf{X}_1, \mathbf{X}_2) = \|\Pi(\mathbf{X}_1) - \Pi(\mathbf{X}_2)\|_F = \|\mathbf{X}_1\mathbf{X}_1^T - \mathbf{X}_2\mathbf{X}_2^T\|_F, \quad (7)$$

as the metric in the induced space. Before explaining our solution, we note that the mapping $\Pi(\cdot)$ and the distance function δ_s are related to the structure of Grassmann manifolds in several aspects. This provides motivation and grounding for the follow-up formulation.

3.1 Properties of the Projection Embedding

The projection embedding $\Pi(\mathbf{X})$ is diffeomorphism from Grassmann manifolds onto the idempotent symmetric matrices with rank p , *i.e.*, it is a one-to-one, continuous, differentiable mapping with a continuous, differentiable inverse (Chikuse 2003). The induced space can be understood as a smooth, compact submanifold of $\text{Sym}(d)$ of dimension $d(d-p)$ (Helmke et al. 2007).

Theorem 1 (Isometry) *The mapping $\Pi(\mathbf{X})$ forms an isometry from $(\mathcal{G}(p, d), \delta_p)$ onto idempotent, rank p subset of $(\text{Sym}(d), \delta_s)$, where the projection distance between two points on the Grassmann manifold $\mathcal{G}(p, d)$ is defined as $\delta_p^2(\mathbf{X}_1, \mathbf{X}_2) = \sum_{i=1}^p \sin^2 \theta_i$ with θ_i representing the principal angles.*

Proof We refer the reader to Chikuse (2003) for the proof of this theorem. \square

Theorem 2 (Length Equivalency) *The length of any given curve is the same under δ_s and δ_g up to a scale of $\sqrt{2}$.*

Proof The proof of this theorem is given in Appendix A. \square

With the above theorems we establish two important properties of the projection embedding which relate distances in the embedding space to Grassmann manifolds. Now we turn our attention to properties of mean in the induced space of $\Pi(\mathbf{X})$. This is important as updating atoms in dictionary learning can be formulated as a weighted mean problem.

Theorem 3 (Closed-Form Mean) *The Karcher (also known as Fréchet) mean for a set of points $\{\mathbf{X}_i\}_{i=1}^N$, $\mathbf{X}_i \in \mathcal{G}(p, d)$ in the embedded space, defined in Eq. (8) below, admits a closed-form solution.*

$$\begin{aligned} \mathbf{X}^* &\triangleq \arg \min_{\mathbf{X}} \sum_{i=1}^N \left\| \mathbf{X} \mathbf{X}^T - \mathbf{X}_i \mathbf{X}_i^T \right\|_F^2, \\ \text{s.t. } &\mathbf{X}^T \mathbf{X} = \mathbf{I}_p, \end{aligned} \quad (8)$$

Proof The proof of this theorem is given in Appendix A. \square

Let $\mathbf{X}_\perp \in \mathbb{R}^{d \times (d-p)}$ be the orthogonal complement of \mathbf{X} , *i.e.*, $\mathbf{X}_\perp^T \mathbf{X} = \mathbf{0}$ and $\mathbf{X}_\perp^T \mathbf{X}_\perp = \mathbf{I}_{d-p}$. Moreover, let the SVD of $\mathbf{X}^T \mathbf{Y}$ and $\mathbf{X}_\perp^T \mathbf{Y}$ be $\mathbf{X}^T \mathbf{Y} = \mathbf{U}_1 \Gamma \mathbf{V}^T$, $\mathbf{X}_\perp^T \mathbf{Y} = -\mathbf{U}_2 \Sigma \mathbf{V}^T$. Here, Γ and Σ are $p \times p$ diagonal matrices with $[\Gamma]_{i,i} = \cos(\theta_i)$ and $[\Sigma]_{i,i} = \sin(\theta_i)$, where θ_i is the i -th principal angle between \mathbf{X} and \mathbf{Y} . Similarly, $\Gamma(\frac{1}{2})$ and $\Sigma(\frac{1}{2})$ are $p \times p$ diagonal matrices with $[\Gamma(\frac{1}{2})]_{i,i} = \cos(\frac{1}{2}\theta_i)$ and $[\Sigma(\frac{1}{2})]_{i,i} = \sin(\frac{1}{2}\theta_i)$. The geometric mean of \mathbf{X} and \mathbf{Y} on the Grassmann manifold denoted by $\mathbf{X} \# \mathbf{Y}$ is given by

$$\mathbf{X} \# \mathbf{Y} = \mathbf{X} \mathbf{U}_1 \Gamma(\frac{1}{2}) - \mathbf{X}_\perp \mathbf{U}_2 \Sigma(\frac{1}{2}). \quad (9)$$

Theorem 4 *The geometric mean of \mathbf{X} and \mathbf{Y} coincides with its Karcher mean in the embedded projection space.*

Proof The proof of this theorem is given in Appendix A. \square

This property resembles a similar property on spheres where the mid-point of a chord when projected back to sphere coincides with the mid-point of an arc.

4 Coding on Grassmann Manifolds

Let \mathbb{D} and \mathbf{X} be a dictionary and a query sample on $\mathcal{G}(p, d)$, respectively. In the following text we discuss how \mathbf{X} can be efficiently represented by a linear combination of atoms in \mathbb{D} . Particularly, we discuss sparse coding and locally linear coding on Grassmann manifolds, and how such codes can be used for classification. The proposed methods are then extended via embedding into Hilbert spaces in Section 5. The problem of learning a dictionary to be used in coding is addressed in Section 6.

4.1 Sparse Coding

Given a dictionary $\mathbb{D} = \{\mathbf{D}_i\}_{i=1}^N$, $\mathbf{D}_i \in \mathcal{G}(p, d)$ and a query sample $\mathbf{X} \in \mathcal{G}(p, d)$, the problem of sparse coding can be expressed as:

$$l(\mathbf{X}, \mathbb{D}) \triangleq \min_{\mathbf{y}} \left\| \mathbf{X} \mathbf{X}^T - \sum_{j=1}^N y_j \mathbf{D}_j \mathbf{D}_j^T \right\|_F^2 + \lambda \|\mathbf{y}\|_1. \quad (10)$$

Expanding the Frobenius norm term in Eq. (10) results in a convex function in \mathbf{y} :

$$\begin{aligned} \left\| \mathbf{X}\mathbf{X}^T - \sum_{j=1}^N y_j \mathbf{D}_j \mathbf{D}_j^T \right\|_F^2 &= \text{Tr}(\mathbf{X}^T \mathbf{X} \mathbf{X}^T \mathbf{X}) + \\ &\sum_{j,r=1}^N y_j y_r \text{Tr}(\mathbf{D}_r^T \mathbf{D}_j \mathbf{D}_j^T \mathbf{D}_r) - 2 \sum_{j=1}^N y_j \text{Tr}(\mathbf{D}_j^T \mathbf{X} \mathbf{X}^T \mathbf{D}_j). \end{aligned}$$

Sparse codes can be obtained without explicit embedding of the manifold to $\text{Sym}(d)$ using $\Pi(\mathbf{X})$. This can be seen by defining $[\mathcal{K}(\mathbf{X}, \mathbb{D})]_i = \text{Tr}(\mathbf{D}_i^T \mathbf{X} \mathbf{X}^T \mathbf{D}_i) = \|\mathbf{X}^T \mathbf{D}_i\|_F^2$ as an N dimensional vector storing the similarity between signal \mathbf{X} and dictionary atoms in the induced space and $[\mathbb{K}(\mathbb{D})]_{i,j} = \text{Tr}(\mathbf{D}_i^T \mathbf{D}_j \mathbf{D}_j^T \mathbf{D}_i) = \|\mathbf{D}_i^T \mathbf{D}_j\|_F^2$ as an $N \times N$ symmetric matrix encoding the similarities between dictionary atoms (which can be computed offline). Then, the sparse coding in Eq. (10) can be written as:

$$l(\mathbf{X}, \mathbb{D}) = \min_{\mathbf{y}} \mathbf{y}^T \mathbb{K}(\mathbb{D}) \mathbf{y} - 2 \mathbf{y}^T \mathcal{K}(\mathbf{X}, \mathbb{D}) + \lambda \|\mathbf{y}\|_1, \quad (11)$$

which is a quadratic problem. The symmetric matrix $\mathbb{K}(\mathbb{D})$ is positive semidefinite as $\forall \mathbf{v} \in \mathbb{R}^N$:

$$\begin{aligned} \mathbf{v}^T \mathbb{K}(\mathbb{D}) \mathbf{v} &= \sum_{i=1}^N \sum_{j=1}^N v_i v_j \text{Tr}(\mathbf{D}_i^T \mathbf{D}_j \mathbf{D}_j^T \mathbf{D}_i) \\ &= \text{Tr} \left(\sum_{i=1}^N \sum_{j=1}^N v_i v_j \mathbf{D}_i \mathbf{D}_i^T \mathbf{D}_j \mathbf{D}_j^T \right) \\ &= \text{Tr} \left(\sum_{i=1}^N v_i \mathbf{D}_i \mathbf{D}_i^T \sum_{j=1}^N v_j \mathbf{D}_j \mathbf{D}_j^T \right) \\ &= \left\| \sum_{i=1}^N v_i \mathbf{D}_i \mathbf{D}_i^T \right\|_F^2 \geq 0. \end{aligned}$$

Therefore, the quadratic problem is convex and can be efficiently solved using common packages like CVX (Grant and Boyd 2012; 2008). We note that the problem in Eq. (11) can be transposed into a vectorized sparse coding problem. More specifically, let $\mathbf{U} \mathbf{\Sigma} \mathbf{U}^T$ be the SVD of $\mathbb{K}(\mathbb{D})$. Then Eq. (11) is equivalent to

$$l(\mathbf{X}, \mathbb{D}) = \min_{\mathbf{y}} \|\mathbf{x}^* - \mathbf{A} \mathbf{y}\|^2 + \lambda \|\mathbf{y}\|_1, \quad (12)$$

where $\mathbf{A} = \mathbf{U} \mathbf{\Sigma}^{1/2}$ and $\mathbf{x}^* = \mathbf{U} \mathbf{\Sigma}^{-1/2} \mathcal{K}(\mathbf{X}, \mathbb{D})$. This could be easily verified by plugging \mathbf{A} and \mathbf{x}^* into Eq. (12). Algorithm 1 provides the pseudo-code for performing Grassmann Sparse Coding (gSC).

We note that for $p = 1$, sparse coding on Grassmann manifolds can be seen as a problem on $d - 1$ dimensional unit sphere, albeit with a subtle difference. More specifically, unlike conventional sparse coding in vector spaces, $\mathbf{x} \sim -\mathbf{x}, \forall \mathbf{x} \in \mathcal{G}(1, d)$, which results in having two hemispheres of the unit sphere being equivalent. For this special case, the solution proposed in Eq. (10) can be understood as sparse

Algorithm 2: Locality-constrained coding on Grassmann manifolds (gLLC).

Input: Grassmann dictionary $\{\mathbf{D}_i\}_{i=1}^N$, $\mathbf{D}_i \in \mathcal{G}(p, d)$; the query sample $\mathbf{X} \in \mathcal{G}(p, d)$
Output: The LLC \mathbf{y}^*
Processing.

```

for  $i \leftarrow 1$  to  $N$  do
  |  $d_i \leftarrow 2p - 2\|\mathbf{D}_i^T \mathbf{X}\|_F^2$ 
end
active_set  $\leftarrow$  indexes of the  $N_{LLC}$  smallest  $d_i, 1 \leq i \leq N$ 
for  $i \leftarrow 1$  to  $N_{LLC}$  do
  |  $\mathbf{B}_i \leftarrow \mathbf{D}_{\text{active\_set}(i)}$ 
end
for  $i, j \leftarrow 1$  to  $N_{LLC}$  do
  |  $[\mathbb{B}]_{i,j} \leftarrow p - \|\mathbf{X}^T \mathbf{B}_i\|_F^2 - \|\mathbf{X}^T \mathbf{B}_j\|_F^2 + \|\mathbf{B}_j^T \mathbf{B}_i\|_F^2$ 
end
Solve the linear equation system  $\mathbb{B}\hat{\mathbf{y}} = \mathbf{1}$ 
 $\hat{\mathbf{y}} \leftarrow \hat{\mathbf{y}}/1^T \hat{\mathbf{y}}$ 
 $\mathbf{y}^*(\text{active\_set}) \leftarrow \hat{\mathbf{y}}$ 

```

$$\min_{\mathbf{y}} \left\| \mathbf{X} \mathbf{X}^T - \sum_{j=1}^{N_{LLC}} y_j \mathbf{B}_j \mathbf{B}_j^T \right\|_F^2 \quad (14)$$

s.t. $\mathbf{1}^T \mathbf{y} = 1.$

A closed-form solution for Eq. (14) can be obtained by forming the Lagrange multiplier to enforce the constraint $\mathbf{1}^T \mathbf{y} = 1$. We note that with the constraint $\mathbf{1}^T \mathbf{y} = 1$

$$\left\| \mathbf{X} \mathbf{X}^T - \sum_{j=1}^{N_{LLC}} y_j \mathbf{B}_j \mathbf{B}_j^T \right\|_F^2 = \left\| \sum_{j=1}^{N_{LLC}} y_j \mathbf{X} \mathbf{X}^T - \sum_{j=1}^{N_{LLC}} y_j \mathbf{B}_j \mathbf{B}_j^T \right\|_F^2 = \mathbf{y}^T \mathbb{B} \mathbf{y}, \quad (15)$$

where $[\mathbb{B}]_{i,j} = p - \|\mathbf{X}^T \mathbf{B}_i\|_F^2 - \|\mathbf{X}^T \mathbf{B}_j\|_F^2 + \|\mathbf{B}_j^T \mathbf{B}_i\|_F^2$. The solution requires an explicit inversion of the matrix \mathbb{B} . In practice, a more efficient solution can be obtained by first solving the linear system of equations, $\mathbb{B}\hat{\mathbf{y}} = \mathbf{1}$, and then to rescale the codes $\hat{\mathbf{y}}$ so that they sum to one (which yields the same result). Algorithm 2 provides the pseudo-code for performing Grassmann Locality-constrained Linear Coding (gLLC).

4.3 Classification Based on Coding

If the atoms in the dictionary are not labeled (*e.g.*, if \mathbb{D} is a generic dictionary not tied to any particular class as will be discussed in § 6), the generated sparse codes (vectors) for both training and query data can be fed to Euclidean-based classifiers like support vector machines (Shawe-Taylor and Cristianini 2004) for classification. In a supervised classification scenario, *i.e.*, if the atoms in sparse

dictionary \mathbb{D} are labeled, the generated codes of the query sample can be directly used for classification. Let $\mathbf{y}_c = [y_0\delta(l(0)-c), y_1\delta(l(1)-c), \dots, y_N\delta(l(N)-c)]^T$ be the class-specific sparse codes, where $l(j)$ is the class label of atom \mathbf{D}_j and $\delta(x)$ is the discrete Dirac function. An efficient way of utilizing class-specific sparse codes is through computing residual errors. In this case, the residual error of query sample $\mathbf{X} \in \mathcal{G}(p, d)$ for class c is defined as:

$$\varepsilon_c(\mathbf{X}) = \left\| \mathbf{X}\mathbf{X}^T - \sum_{j=1}^N y_j \mathbf{D}_j \mathbf{D}_j^T \delta(l(j) - c) \right\|_F^2. \quad (16)$$

Alternatively, the similarity between query sample \mathbf{X} to class c can be defined as $s(\mathbf{X}, c) = h(\mathbf{y}_c)$. The function $h(\cdot)$ could be a linear function like $\sum_{j=1}^N (\cdot)$ or even a non-linear one like $\max(\cdot)$. Preliminary experiments suggest that Eq. (16) leads to higher classification accuracies when compared to the aforementioned alternatives.

4.4 Extrinsic Nature of the Solution

The solutions proposed in this section (*e.g.*, Eq. (10)) consider $\Pi(\mathbf{X})$ as a mapping and solve sparse coding extrinsically, meaning $\sum_i [\mathbf{y}]_i \mathbf{D}_i \mathbf{D}_i^T$ is not necessarily a point on $\mathcal{G}(p, d)$. If, however, it is required that the linear combination of elements $\sum_i [\mathbf{y}]_i \mathbf{D}_i \mathbf{D}_i^T$ actually be used to represent a point on a Grassmann manifold, it can be accomplished as follows. The **Eckart-Young** theorem (Golub and Van Loan 1996) states that the matrix of rank p closest in Frobenius norm to a given matrix \mathbf{X} is found by dropping all the singular values beyond the p -th value. This operation (along with equalization of the singular values) can be easily applied to a linear combination of matrices $\mathbf{D}_i \mathbf{D}_i^T$ to obtain a point on the manifold. Thus, in a very concrete sense, the linear combination of elements $\mathbf{D}_i \mathbf{D}_i^T$, although not equaling any point on the Grassmann manifold, does *represent* such an element, the closest point lying on the manifold itself.

Furthermore, the proposed methods follow the general principle of coding in that the over-completeness of \mathbb{D} will approximate $\mathbf{X}\mathbf{X}^T$ and $\sum_i [\mathbf{y}]_i \mathbf{D}_i \mathbf{D}_i^T$ could be safely expected to be closely tied to a Grassmann point. Since $d \times d$ symmetric matrices of rank p with the extra property of being idempotent² are equivalent to points on $\mathcal{G}(p, d)$, an intrinsic version of Eq. (10) can be written as:

$$\min_{\mathbf{y}} \left\| \mathbf{X}\mathbf{X}^T - \text{Proj} \left(\sum_{j=1}^N [\mathbf{y}]_j \mathbf{D}_j \mathbf{D}_j^T \right) \right\|_F^2 + \lambda \|\mathbf{y}\|_1, \quad (17)$$

where $\text{Proj}(\cdot)$ is the operator that projects a symmetric matrix onto a Grassmann manifold (by forcing the idempotency and rank properties). Based on the Eckart-Young theorem, $\text{Proj}(\cdot)$ can be obtained through SVD. The involvement of SVD, especially in vision applications, makes solving Eq. (17) tedious and challenging. We acknowledge that seeking efficient ways of solving Eq. (17) is interesting but beyond the scope of this work.

² A matrix \mathbf{P} is called idempotent if $\mathbf{P}^2 = \mathbf{P}$.

5 Kernelized Coding on Grassmann Manifolds

In this section, we are interested in coding on higher-dimensional (possibly infinite-dimensional) Grassmann manifolds. Such treatment is helpful in dealing with non-linearity of data since one can hope higher-dimensional manifolds diminish non-linearity. To this end, we make use of a mapping $\phi : \mathbb{R}^d \rightarrow \mathcal{H}$ from \mathbb{R}^d into a dot product Hilbert space \mathcal{H} with a real-valued reproducing kernel function $k(\cdot, \cdot)$ on $\mathbb{R}^d \times \mathbb{R}^d$, such that $\forall \mathbf{x}, \mathbf{x}' \in \mathbb{R}^d$, $\langle \mathbf{x}, \mathbf{x}' \rangle_{\mathcal{H}} = \phi(\mathbf{x})^T \phi(\mathbf{x}') = k(\mathbf{x}, \mathbf{x}')$ (Shawe-Taylor and Cristianini 2004).

Our goal here is to perform both sparse coding and locally linear coding in \mathcal{H} , but for efficiency we want to avoid explicitly working in \mathcal{H} . In other words, we would like to obtain sparse or locally linear codes by only using $k(\cdot, \cdot)$. In the following text we elaborate how this can be achieved.

5.1 Kernel Sparse Coding

Let $\Psi_{\mathbf{X}} = [\psi_1 | \psi_2 | \dots | \psi_p]$ be an orthonormal basis of order p for the column space of $\Phi_{\mathbf{X}} = [\phi(\mathbf{x}_1) | \phi(\mathbf{x}_2) | \dots | \phi(\mathbf{x}_q)]$, $p \leq q$ in \mathcal{H} . We note that the $q \times q$ Gram matrix $\Phi^T(\mathbf{X})\Phi(\mathbf{X})$ whose i^{th} row and j^{th} column entry is $k(\mathbf{x}_i, \mathbf{x}_j)$ can be decomposed as:

$$\Phi_{\mathbf{X}}^T \Phi_{\mathbf{X}} = U_{\mathbf{X}} \Sigma_{\mathbf{X}} U_{\mathbf{X}}^T. \quad (18)$$

The connection between $U_{\mathbf{X}}$ and $\Psi_{\mathbf{X}}$ is a well-known ‘‘trick’’ used to compute the principal components of a matrix that has considerably less columns than rows (Turk and Pentland 1991), and can be easily established as:

$$\Psi_{\mathbf{X}} = \Phi_{\mathbf{X}} U_{\mathbf{X}} \Sigma_{\mathbf{X}}^{-1/2}. \quad (19)$$

The sparse coding problem on a Grassmann manifold embedded in \mathcal{H}^p can be understood as the kernel version of Eq. (11), as depicted below:

$$\min_{\mathbf{y}} \left\| \Psi_{\mathbf{X}} \Psi_{\mathbf{X}}^T - \sum_{j=1}^N y_j \Psi_{D_j} \Psi_{D_j}^T \right\|_F^2 + \lambda \|\mathbf{y}\|_1. \quad (20)$$

A similar statement to what we have in § 4.1 holds here for the convexity of Eq. (20). Therefore, sparse codes can be obtained if the Frobenius norms between $\Psi_{\mathbf{X}}$ and elements of the dictionary, *i.e.*, $\{\Psi_{D_i}\}_{i=1}^N$ are known. Given $\{\mathbf{z}_i\}_{i=1}^{q_Z}$, $\mathbf{z}_i \in \mathbb{R}^d$ and $\{\mathbf{x}_i\}_{i=1}^{q_X}$, $\mathbf{x}_i \in \mathbb{R}^d$, the Frobenius norm between the corresponding subspaces $\Psi_{\mathbf{Z}}$ and $\Psi_{\mathbf{X}}$ in \mathcal{H}^p can be obtained as:

$$\begin{aligned} \left\| \Psi_{\mathbf{Z}}^T \Psi_{\mathbf{X}} \right\|_F^2 &= \left\| \Sigma_{\mathbf{Z}}^{-1/2} U_{\mathbf{Z}}^T \Phi_{\mathbf{Z}}^T \Phi_{\mathbf{X}} U_{\mathbf{X}} \Sigma_{\mathbf{X}}^{-1/2} \right\|_F^2 \\ &= \left\| \Sigma_{\mathbf{Z}}^{-1/2} U_{\mathbf{Z}}^T \mathbf{K}(\mathbf{Z}, \mathbf{X}) U_{\mathbf{X}} \Sigma_{\mathbf{X}}^{-1/2} \right\|_F^2, \end{aligned} \quad (21)$$

where $\mathbf{K}(\mathbf{Z}, \mathbf{X})$ is a $q_Z \times q_X$ matrix whose i -th row and j -th column entry is $k(\mathbf{z}_i, \mathbf{x}_j)$. Therefore, a similar approach to § 4.1 can be employed to obtain the sparse codes in Eq. (20). Algorithm 3 provides the pseudo-code for performing kernel sparse coding on Grassmann manifolds (kgSC).

Algorithm 3: Kernel sparse coding on Grassmann manifolds (kgSC).

Input: Grassmann dictionary $\{\mathbf{D}_i\}_{i=1}^N \in \mathbb{R}^{d \times q_i}$ with $\mathbf{D}_i = \{\mathbf{d}_{i,j}\}_{j=1}^{q_i}$, $\mathbf{d}_{i,j} \in \mathbb{R}^d$;
the query sample $\mathbf{X} \in \mathbb{R}^{d \times q}$

Output: The sparse code \mathbf{y}^*

Initialization.

```

for  $i \leftarrow 1$  to  $N$  do
   $[\mathbf{K}(\mathbf{D}_i)]_{j,l} \leftarrow k(\mathbf{d}_{i,j}, \mathbf{d}_{i,l})$ 
   $\mathbf{K}(\mathbf{D}_i) = \mathbf{U}_{\mathbf{D}_i} \boldsymbol{\Sigma}_{\mathbf{D}_i} \mathbf{U}_{\mathbf{D}_i}^T$ ; /* SVD of  $\mathbf{K}(\mathbf{D}_i)$  */
end
for  $i, j \leftarrow 1$  to  $N$  do
   $[\mathbb{K}(\mathbb{D})]_{i,j} \leftarrow \left\| \boldsymbol{\Sigma}_{\mathbf{D}_j}^{-1/2} \mathbf{U}_{\mathbf{D}_j}^T \mathbf{K}(\mathbf{D}_j, \mathbf{D}_i) \mathbf{U}_{\mathbf{D}_i} \boldsymbol{\Sigma}_{\mathbf{D}_i}^{-1/2} \right\|_F^2$ 
end
 $\mathbb{K}(\mathbb{D}) = \mathbf{U} \boldsymbol{\Sigma} \mathbf{U}^T$  /* compute SVD of  $\mathbb{K}(\mathbb{D})$  */
 $\mathbf{A} \leftarrow \mathbf{U} \boldsymbol{\Sigma}^{1/2}$ 

```

Processing.

```

 $[\mathbf{K}(\mathbf{X})]_{i,j} \leftarrow k(\mathbf{x}_i, \mathbf{x}_j)$ ;
 $\mathbf{K}(\mathbf{X}) = \mathbf{U}_{\mathbf{X}} \boldsymbol{\Sigma}_{\mathbf{X}} \mathbf{U}_{\mathbf{X}}^T$ ; /* SVD of  $\mathbf{K}(\mathbf{X})$  */
for  $i \leftarrow 1$  to  $N$  do
   $[\mathbf{K}(\mathbf{X}, \mathbf{D}_i)]_{j,l} \leftarrow k(\mathbf{x}_j, \mathbf{d}_{i,l})$ 
   $[\mathcal{K}(\mathbf{X}, \mathbb{D})]_i \leftarrow \left\| \boldsymbol{\Sigma}_{\mathbf{X}}^{-1/2} \mathbf{U}_{\mathbf{X}}^T \mathbf{K}(\mathbf{X}, \mathbf{D}_i) \mathbf{U}_{\mathbf{D}_i} \boldsymbol{\Sigma}_{\mathbf{D}_i}^{-1/2} \right\|_F^2$ 
end
 $\mathbf{x}^* \leftarrow \mathbf{U} \boldsymbol{\Sigma}^{-1/2} \mathcal{K}(\mathbf{X}, \mathbb{D})$ 
 $\mathbf{y}^* \leftarrow \arg \min_{\mathbf{y}} \|\mathbf{x}^* - \mathbf{A} \mathbf{y}\|^2 + \lambda \|\mathbf{y}\|_1$ 

```

5.2 Kernel Locality-Constrained Linear Coding

Based on the development in §5.1, the kernel version of LLC algorithm on Grassmann manifolds can be obtained readily. To this end, we need to rewrite Eq. (14) in Hilbert space as follows:

$$\min_{\mathbf{y}} \left\| \boldsymbol{\Psi}_{\mathbf{X}} \boldsymbol{\Psi}_{\mathbf{X}}^T - \sum_{j=1}^{N_{LLC}} y_j \boldsymbol{\Psi}_{\mathbf{B}_j} \boldsymbol{\Psi}_{\mathbf{B}_j}^T \right\|_F^2 \quad (22)$$

s.t. $\mathbf{1}^T \mathbf{y} = 1.$

A closed-form solution for Eq. (22) can be obtained similar to §5.1. We note that with the constraint $\mathbf{1}^T \mathbf{y} = 1$

$$\left\| \boldsymbol{\Psi}_{\mathbf{X}} \boldsymbol{\Psi}_{\mathbf{X}}^T - \sum_{j=1}^{N_{LLC}} y_j \boldsymbol{\Psi}_{\mathbf{B}_j} \boldsymbol{\Psi}_{\mathbf{B}_j}^T \right\|_F^2 = \mathbf{y}^T \mathbb{B}_{\mathcal{H}} \mathbf{y},$$

Algorithm 4: Kernel locality-constrained linear coding on Grassmann manifolds (kgLLC).

Input: Grassmann dictionary $\{\mathbf{D}_i\}_{i=1}^N$, $\mathbf{D}_i \in \mathcal{G}(p, d)$; the query sample $\mathbf{X} \in \mathcal{G}(p, d)$
Output: The LLC \mathbf{y}^*

Processing.

```

for  $i \leftarrow 1$  to  $N$  do
  |  $d_i \leftarrow 2p - 2 \left\| \boldsymbol{\Sigma}_{\mathbf{D}_i}^{-1/2} \mathbf{U}_{\mathbf{D}_i}^T \mathbf{K}(\mathbf{D}_i, \mathbf{X}) \mathbf{U}_{\mathbf{X}} \boldsymbol{\Sigma}_{\mathbf{X}}^{-1/2} \right\|_F^2$ 
end
active.set  $\leftarrow$  indexes of the  $N_{LLC}$  smallest  $d_i, 1 \leq i \leq N$ 
for  $i \leftarrow 1$  to  $N_{LLC}$  do
  |  $\mathbf{B}_i \leftarrow \mathbf{D}_{\text{active.set}(i)}$ 
end
for  $i, j \leftarrow 1$  to  $N_{LLC}$  do
  | Compute  $[\mathbb{B}_{\mathcal{H}}]_{i,j}$  using (23)
end
Solve the linear equation system  $\mathbb{B}_{\mathcal{H}} \hat{\mathbf{y}} = \mathbf{1}$ 
 $\hat{\mathbf{y}} \leftarrow \hat{\mathbf{y}} / \mathbf{1}^T \hat{\mathbf{y}}$ 
 $\mathbf{y}^*(\text{active.set}) \leftarrow \hat{\mathbf{y}}$ 

```

where

$$\begin{aligned}
[\mathbb{B}_{\mathcal{H}}]_{i,j} &= p - \left\| \boldsymbol{\Psi}_{\mathbf{X}}^T \boldsymbol{\Psi}_{\mathbf{B}_i} \right\|_F^2 - \left\| \boldsymbol{\Psi}_{\mathbf{X}}^T \boldsymbol{\Psi}_{\mathbf{B}_j} \right\|_F^2 + \left\| \boldsymbol{\Psi}_{\mathbf{B}_j}^T \boldsymbol{\Psi}_{\mathbf{B}_i} \right\|_F^2 \\
&= p - \left\| \boldsymbol{\Sigma}_{\mathbf{B}_i}^{-1/2} \mathbf{U}_{\mathbf{B}_i}^T \mathbf{K}(\mathbf{B}_i, \mathbf{X}) \mathbf{U}_{\mathbf{X}} \boldsymbol{\Sigma}_{\mathbf{X}}^{-1/2} \right\|_F^2 \\
&\quad - \left\| \boldsymbol{\Sigma}_{\mathbf{B}_j}^{-1/2} \mathbf{U}_{\mathbf{B}_j}^T \mathbf{K}(\mathbf{B}_j, \mathbf{X}) \mathbf{U}_{\mathbf{X}} \boldsymbol{\Sigma}_{\mathbf{X}}^{-1/2} \right\|_F^2 \\
&\quad + \left\| \boldsymbol{\Sigma}_{\mathbf{B}_i}^{-1/2} \mathbf{U}_{\mathbf{B}_i}^T \mathbf{K}(\mathbf{B}_i, \mathbf{B}_j) \mathbf{U}_{\mathbf{B}_j} \boldsymbol{\Sigma}_{\mathbf{B}_j}^{-1/2} \right\|_F^2.
\end{aligned} \tag{23}$$

The solution is obtained by first solving the linear system of equations, $\mathbb{B}_{\mathcal{H}} \hat{\mathbf{y}} = \mathbf{1}$, and then to rescale the codes $\hat{\mathbf{y}}$ so that they sum to one. Algorithm 4 provides the pseudo-code for performing kernel locality-constrained linear coding on Grassmann manifolds (kgLLC).

6 Dictionary Learning

Given a finite set of observations $\mathbb{X} = \{\mathbf{x}_i\}_{i=1}^m$, $\mathbf{x}_i \in \mathcal{G}(p, d)$, the problem of dictionary learning on Grassmann manifolds is defined as:

$$h(\mathbb{D}) \triangleq \sum_{i=1}^m l_{\mathcal{G}}(\mathbf{x}_i, \mathbb{D}), \tag{24}$$

with $\mathbb{D} = [\mathbf{D}_1 | \mathbf{D}_2 | \dots | \mathbf{D}_N]$ being a dictionary of size N with atoms $\mathbf{D}_i \in \mathcal{G}(p, d)$. Here, $l_{\mathcal{G}}(\mathbf{x}, \mathbb{D})$ is a loss function and should be small if \mathbb{D} is “good” at representing the signal \mathbf{x} . In the following text we first elaborate on how Grassmann dictionaries can be obtained by taking into account sparsity. We then discuss the kernel extension which can account for higher-dimensional Grassmann manifolds. Finally, we introduce optimum dictionaries for locality-constrained linear coding.

6.1 Dictionary Learning for Sparse Coding

Aiming for sparsity, the ℓ_1 -norm regularization is usually employed to obtain the most common form of $l_G(\mathbf{X}, \mathbb{D})$ as depicted in Eq. (10). With this choice, finding the optimum \mathbb{D} in Eq. (24) is not trivial because of non-convexity, as can be seen by rewriting the dictionary learning to:

$$\min_{\{\mathbf{y}_i\}_{i=1}^m, \mathbb{D}} \sum_{i=1}^m \left\| \mathbf{X}_i \mathbf{X}_i^T - \sum_{j=1}^N [\mathbf{y}_i]_j \mathbf{D}_j \mathbf{D}_j^T \right\|_F^2 + \lambda \sum_{i=1}^m \|\mathbf{y}_i\|_1. \quad (25)$$

A common approach to solving this is to alternate between the two sets of variables, \mathbb{D} and $\mathbf{Y} = [\mathbf{y}_1 | \mathbf{y}_2 | \dots | \mathbf{y}_m]$, as proposed for example by Elad (2010). More specifically, minimizing Eq. (25) over sparse codes \mathbf{y} while dictionary \mathbb{D} is fixed is a convex problem. Similarly, minimizing the overall problem over \mathbb{D} with fixed $\{\mathbf{y}_i\}_{i=1}^m$ is convex as well.

Therefore, to update dictionary atoms we break the minimization problem into N sub-minimization problems by independently updating each atom, in line with general practice in dictionary learning (Elad 2010). More specifically, fixing sparse codes and ignoring the terms that are irrelevant to dictionary atoms, the dictionary learning problem can be seen as finding $\min_{\mathbb{D}} \sum_{r=1}^N \mathcal{J}(r)$, where:

$$\mathcal{J}(r) = \sum_{i=1}^m \sum_{j=1, j \neq r}^N [\mathbf{y}_i]_r [\mathbf{y}_i]_j \text{Tr}(\mathbf{D}_r^T \mathbf{D}_j \mathbf{D}_j^T \mathbf{D}_r) - 2 \sum_{i=1}^m [\mathbf{y}_i]_r \text{Tr}(\mathbf{D}_r^T \mathbf{X}_i \mathbf{X}_i^T \mathbf{D}_r). \quad (26)$$

Imposing the orthogonality of \mathbf{D}_r results in the following minimization sub-problem for updating \mathbf{D}_r :

$$\begin{aligned} \mathbf{D}_r^* &= \underset{\mathbf{D}_r}{\text{argmin}} \mathcal{J}(r), \\ \text{s.t. } & \mathbf{D}_r^T \mathbf{D}_r = \mathbf{I}_p. \end{aligned} \quad (27)$$

A closed-form solution for the above minimization problem can be obtained by the method of Lagrange multipliers and forming $L(r, \zeta) = \mathcal{J}(r) + \zeta (\mathbf{D}_r^T \mathbf{D}_r - \mathbf{I}_p)$. The gradient of $L(r, \zeta)$ is:

$$\nabla_{\mathbf{D}_r} L(r, \zeta) = 2 \sum_{i=1}^m \sum_{j=1, j \neq r}^N [\mathbf{y}_i]_r [\mathbf{y}_i]_j \mathbf{D}_j \mathbf{D}_j^T \mathbf{D}_r - 4 \sum_{i=1}^m [\mathbf{y}_i]_r \mathbf{X}_i \mathbf{X}_i^T \mathbf{D}_r + 2\zeta \mathbf{D}_r. \quad (28)$$

The solution of Eq. (27) can be sought by finding the roots of Eq. (28), *i.e.*, $\nabla_{\mathbf{D}_r} L(r, \zeta) = 0$, which is an eigen-value problem. Therefore, the solution of Eq. (27) can be obtained by computing p eigenvectors of \mathcal{S} , where

$$\mathcal{S} = \sum_{i=1}^m \sum_{j=1, j \neq r}^N [\mathbf{y}_i]_r [\mathbf{y}_i]_j \mathbf{D}_j \mathbf{D}_j^T - 2 \sum_{i=1}^m [\mathbf{y}_i]_r \mathbf{X}_i \mathbf{X}_i^T. \quad (29)$$



Fig. 3: (a) Examples of actions performed by a ballerina. (b) The dominant eigenvectors for four atoms learned by the proposed Grassmann Dictionary Learning (gDL) method (grayscale images were used in gDL).

To perform coding, we have relaxed the rank constraint of the mapping $\Pi(\mathbf{X})$ since matrix addition and subtraction do not preserve the matrix rank. However, for dictionary learning, the orthogonality constraint ensures the dictionary atoms have the required rank. This is in spirit similar to coding and dictionary learning in vector spaces. More specifically, consider sparse coding in \mathbb{R}^d with unit-length query signal and dictionary. While both query and dictionary atoms are points on a unit $d-1$ hypersphere, the sparse linear combination of atoms that approximates the query signal does not necessarily result in a point on the hypersphere.

Note that the mapping $\Pi(\mathbf{X})$ meets the requirement of a Grassmann kernel (Hamm and Lee 2008). Consequently, it is possible to interpret the above solution as a kernel method. Nevertheless, we believe that the explanation through manifold of symmetric matrices provides more insight into the solution and also avoids possible confusion with the following section, where we present an explicitly kernelized version of Grassmann Dictionary Learning (gDL). Fig. 3 shows examples of a ballet dance and the atoms learned by the proposed gDL method. From each atom, we plot the dominant eigendirection because it is visually more informative. Note that the learned atoms capture the ballerina movements.

6.2 Kernel Dictionary Learning for Sparse Coding

Similar to the linear gDL method, dictionary is updated atom by atom (*i.e.*, atoms are assumed to be independent) by fixing sparse codes. As such, the cost function to update $\Psi(\mathbf{D}_r)$ can be defined as:

Algorithm 5: Grassmann Dictionary Learning (gDL)

Input: training set $\mathbb{X} = \{\mathbf{X}_i\}_{i=1}^m$ from the underlying Grassmann manifold, where each $\mathbf{X}_i \in \mathcal{G}_{d,p}$ is a subspace of order p in \mathbb{R}^d ; $nIter$, number of iterations

Output: Grassmann dictionary $\mathbb{D} = \{\mathbf{D}_i\}_{i=1}^N$

Initialization.

| Initialize the dictionary $\mathbb{D} = \{\mathbf{D}_i\}_{i=1}^N$ by selecting N samples from \mathbb{X} randomly

Processing.

```

for  $t = 1$  to  $nIter$  do
  /* Sparse Coding Step using Algorithm 1 */
  for  $i = 1$  to  $m$  do
     $\mathbf{y}_i \leftarrow \min_{\mathbf{y}} \|\mathbf{X}\mathbf{X}^T - \sum_{j=1}^N y_j \mathbf{D}_j \mathbf{D}_j^T\|_F^2 + \lambda \|\mathbf{y}\|_1$ 
  end
  /* Dictionary update step */
  for  $r = 1$  to  $N$  do
     $\mathbf{S} \leftarrow \sum_{i=1}^m y_{i,r} \left( \sum_{j=1, j \neq r}^N y_{i,j} \mathbf{D}_j \mathbf{D}_j^T - \mathbf{X}_i \mathbf{X}_i^T \right)$ 
     $\{\tilde{\lambda}_k, \tilde{\mathbf{v}}_k\} \leftarrow$  eigenvalues and eigenvectors of  $\mathbf{S}$ 
     $\mathbf{S}\tilde{\mathbf{v}} = \tilde{\lambda}\tilde{\mathbf{v}}; \tilde{\lambda}_1 \leq \tilde{\lambda}_2 \leq \dots \leq \tilde{\lambda}_d$ 
     $\mathbf{D}_r^* \leftarrow [\tilde{\mathbf{v}}_1 | \tilde{\mathbf{v}}_2 | \dots | \tilde{\mathbf{v}}_p]$ 
  end
end

```

$$\begin{aligned}
\mathcal{J}_{\Psi}(r) &= \sum_{i,j} [\mathbf{y}_i]_r [\mathbf{y}_i]_j \text{Tr}(\Psi(\mathbf{D}_r)^T \Psi(\mathbf{D}_j) \Psi(\mathbf{D}_j)^T \Psi(\mathbf{D}_r)) \\
&\quad - 2 \sum_{i=1}^m [\mathbf{y}_i]_r \text{Tr}(\Psi(\mathbf{D}_r)^T \Psi(\mathbf{X}_i) \Psi(\mathbf{X}_i)^T \Psi(\mathbf{D}_r)), \\
&= \sum_{i=1}^m \sum_{j=1, j \neq r}^N [\mathbf{y}_i]_r [\mathbf{y}_i]_j \text{Tr}(\mathbf{A}_{\mathbf{D}_r}^T \mathbf{B}(\mathbf{D}_r, \mathbf{D}_j) \mathbf{A}_{\mathbf{D}_r}) \\
&\quad - 2 \sum_{i=1}^m [\mathbf{y}_i]_r \text{Tr}(\mathbf{A}_{\mathbf{D}_r}^T \mathbf{B}(\mathbf{D}_r, \mathbf{X}_i) \mathbf{A}_{\mathbf{D}_r}), \tag{30}
\end{aligned}$$

where $\mathbf{B}(\mathbf{X}, \mathbf{Z}) = \mathbf{K}(\mathbf{X}, \mathbf{Z}) \mathbf{A}_{\mathbf{Z}} \mathbf{A}_{\mathbf{Z}}^T \mathbf{K}(\mathbf{Z}, \mathbf{X})$. The orthogonality constraint in \mathcal{H} can be written as:

$$\Psi(\mathbf{D}_r)^T \Psi(\mathbf{D}_r) = \mathbf{A}_{\mathbf{D}_r}^T \mathbf{K}(\mathbf{D}_r, \mathbf{D}_r) \mathbf{A}_{\mathbf{D}_r} = \mathbf{I}_p. \tag{31}$$

$\Psi(\mathbf{D}_r)$ is fully determined if $\mathbf{A}_{\mathbf{D}_r}$ and $\mathbf{K}(\cdot, \mathbf{D}_r)$ are known. If we assume that dictionary atoms are independent, then according to the representer theorem (Shawe-Taylor and Cristianini 2004), $\Psi(\mathbf{D}_r)$ is a linear combination of all the \mathbf{X}_i that have used it. Therefore, $\mathbf{K}(\cdot, \mathbf{D}_r) = \mathbf{K}(\cdot, \bigcup_i \mathbf{X}_i)$, $y_{i,r} \neq 0$ which leaves us with identify-

ing \mathbf{A}_{D_r} via the following minimization problem:

$$\begin{aligned} \min_{\mathbf{A}_{D_r}} & \sum_{i=1}^m \sum_{j=1, j \neq r}^N y_{i,r} y_{i,j} \text{Tr}(\mathbf{A}_{D_r}^T \mathbf{B}(\mathbf{D}_r, \mathbf{D}_j) \mathbf{A}_{D_r}) \\ & - 2 \sum_{i=1}^m y_{i,r} \text{Tr}(\mathbf{A}_{D_r}^T \mathbf{B}(\mathbf{D}_r, \mathbf{X}_i) \mathbf{A}_{D_r}) \\ \text{s.t.} & \mathbf{A}_{D_r}^T \mathbf{K}(\mathbf{D}_r, \mathbf{D}_r) \mathbf{A}_{D_r} = \mathbf{I}_p. \end{aligned}$$

The solution of the above problem is given by the eigenvectors of the generalized eigenvalue problem $\mathcal{S}_\Psi \mathbf{v} = \lambda \mathbf{K}(\mathbf{D}_r, \mathbf{D}_r) \mathbf{v}$, where:

$$\mathcal{S}_\Psi = \sum_{i=1}^m [\mathbf{y}_i]_r \left(\sum_{j=1, j \neq r}^N [\mathbf{y}_i]_j \mathbf{B}(\mathbf{D}_r, \mathbf{D}_j) - 2 \mathbf{B}(\mathbf{D}_r, \mathbf{X}_i) \right). \quad (32)$$

All of the above details for the Kernel Grassmann Dictionary Learning (kgDL) approach are combined in Algorithm 6.

6.3 Dictionary Learning for LLC Coding

Similar to §6.1, learning a dictionary \mathbb{D} for gLLC can be formulated as:

$$\begin{aligned} \min_{\{\mathbf{y}_i\}_{i=1}^m, \mathbb{D}} & \sum_{i=1}^m \left\| \mathbf{X}_i \mathbf{X}_i^T - \sum_{j=1}^{N_{LLC}} [\mathbf{y}_i]_j \mathbf{B}_{i,j} \mathbf{B}_{i,j}^T \right\|_F^2 \\ \text{s.t.} & \mathbf{1}^T \mathbf{y}_i = 1, \quad 1 \leq i \leq m, \end{aligned} \quad (33)$$

where $\mathbf{B}_{i,j} \in \mathbb{D}$, $1 \leq j \leq N_{LLC}$ is a local basis for training data \mathbf{X}_i , *i.e.*, $\mathbf{B}_{i,j}$ is a set of N_{LLC} closest dictionary atoms to \mathbf{X}_i . The gLLC dictionary can be obtained by alternating between the two sets of variables, \mathbb{D} and $\mathbf{Y} = [\mathbf{y}_1 | \mathbf{y}_2 | \dots | \mathbf{y}_m]$ of Eq. (33). We note that in terms of updating the dictionary atoms, the derivation provided in §6.1 can be seamlessly used to update the dictionary atoms. More specifically, the p smallest eigenvectors of Eq. (29) provide the update for \mathbf{D}_r , where \mathbf{y}_i are obtained through the gLLC algorithm. A similar argument holds for the kernel version of gLLC and atoms can be updated through Eq. (32).

7 Experiments

Two sets of experiments³ are presented in this section. In the first set of experiments, we evaluate the performance of the proposed methods (as described in §4 and §5) without dictionary learning. This is to contrast proposed coding schemes to previous state-of-the-art methods on several popular closed-set classification tasks. To this end, each point in the training set is considered as an atom in the dictionary. Since the atoms in the dictionary are labeled in this case, the residual error approach for classification (as described in §4.3) will be used to determine the label of a query point. In the second set of experiments, the performance of the

³ Matlab/Octave source code is available at <http://itee.uq.edu.au/~uqmharal>

Algorithm 6: Kernelized Grassmann Dictionary Learning (kgDL)

Input: training set $\mathbb{X} = \{\mathbf{X}_i\}_{i=1}^{m_i}$, where $\mathbf{X}_i \in \mathbb{R}^{d \times m_i}$; $k(\cdot, \cdot)$, a kernel function; $nIter$, the number of iterations.

Output: Grassmann dictionary represented by $\mathbb{A} = \{\mathbf{A}_{D_i}\}_{i=1}^N$ and $\mathbb{K} = \{\mathbf{K}(\cdot, \mathbf{D}_i)\}_{i=1}^N$

Initialization.

Initialize the dictionary $\mathbb{D} = \{\mathbf{D}_i\}_{i=1}^N$ by selecting N samples from \mathbb{X} randomly;
 Compute $\{\mathbf{A}_{X_i}\}_{i=1}^m$ for all points in \mathbb{X} using KPCA algorithm;
 Compute $\{\mathbf{A}_{D_i}\}_{i=1}^N$ for all points in \mathbb{D} using KPCA algorithm;
 $\mathbf{\Gamma} \leftarrow \mathbf{0}_{N \times N}$;
 $\boldsymbol{\gamma} \leftarrow \mathbf{0}_{N \times 1}$;

Processing.

```

for  $t = 1$  to  $nIter$  do
  /* Sparse Coding Step */
  for  $i, j = 1$  to  $N$  do
     $[\mathbf{\Gamma}]_{i,j} \leftarrow \text{Tr}(\mathbf{A}_{D_i}^T \mathbf{K}(\mathbf{D}_i, \mathbf{D}_j) \mathbf{A}_{D_j} \mathbf{A}_{D_j}^T \mathbf{K}(\mathbf{D}_j, \mathbf{D}_i) \mathbf{A}_{D_i})$ ;
  end
  for  $i = 1$  to  $m$  do
    for  $j = 1$  to  $N$  do
       $[\boldsymbol{\gamma}]_j \leftarrow \text{Tr}(\mathbf{A}_{D_j}^T \mathbf{K}(\mathbf{D}_j, \mathbf{X}_i) \mathbf{A}_{X_i} \mathbf{A}_{X_i}^T \mathbf{K}(\mathbf{D}_j, \mathbf{X}_i) \mathbf{A}_{D_j})$ ;
    end
     $\mathbf{y}_i \leftarrow \underset{\mathbf{y}}{\text{argmin}} \mathbf{y}^T \mathbf{\Gamma} \mathbf{y} - 2\mathbf{y}^T \boldsymbol{\gamma} + Sp(\mathbf{y})$ ;
  end
  /* Dictionary update step */
  for  $r = 1$  to  $N$  do
     $\mathbf{K}(\cdot, \mathbf{D}_r) \leftarrow \mathbf{K}(\cdot, \bigcup_{i, y_{i,r} \neq 0} \mathbf{X}_i)$ ;
     $\mathbf{S}_{\Psi} \leftarrow \sum_{i=1}^m \sum_{j \neq r} y_{i,r} y_{i,j} \mathbf{K}(\mathbf{D}_r, \mathbf{D}_j) \mathbf{A}_{D_j} \mathbf{A}_{D_j}^T \mathbf{K}(\mathbf{D}_j, \mathbf{D}_r)$ 
       $- 2 \sum_{i=1}^m y_{i,r} \mathbf{K}(\mathbf{D}_r, \mathbf{X}_i) \mathbf{A}_{X_i} \mathbf{A}_{X_i}^T \mathbf{K}(\mathbf{X}_i, \mathbf{D}_r)$ ;
     $\{\tilde{\lambda}_k, \tilde{\mathbf{v}}_k\} \leftarrow$  generalized eigenvalues and eigenvectors of
     $\mathbf{S}_{\Psi} \tilde{\mathbf{v}} = \tilde{\lambda} \mathbf{K}(\mathbf{D}_r, \mathbf{D}_r) \tilde{\mathbf{v}}$ ;  $\tilde{\lambda}_1 \leq \tilde{\lambda}_2 \leq \dots \leq \tilde{\lambda}_d$ ;
     $\mathbf{A}_{D_r}^* \leftarrow [\tilde{\mathbf{v}}_1 | \tilde{\mathbf{v}}_2 | \dots | \tilde{\mathbf{v}}_p]$ ;
  end
end

```

coding methods is evaluated in conjunction with the proposed dictionary learning algorithms described in § 6. Before delving into experiments, we discuss how videos and image-sets can be modeled by linear subspaces and hence as points on Grassmann manifolds.

7.1 Representing Image-Sets and Videos on Grassmann Manifolds

Let us define a video as an ordered collection of images with time-stamp information, and an image-set as simply an orderless collection of images. In this section we briefly demonstrate how videos and image-sets can be modeled by subspaces (and hence as points on Grassmann manifolds). We first consider approaches where the

time-stamp information is ignored, followed by an approach where the dynamics of image sequences are taken into account.

7.1.1 Modeling of Appearance

The appearance of an image-set or video $\mathbb{F} = \{\mathbf{f}_1, \mathbf{f}_2, \dots, \mathbf{f}_\tau\}$, where $\mathbf{f}_i \in \mathbb{R}^d$ is the vectorized representation of i -th observation (frame in video), can be represented by a linear subspace through any orthogonalization procedure like SVD. More specifically, let $\mathbf{U}\mathbf{\Sigma}\mathbf{V}^T$ be the SVD of \mathbb{F} . The first p columns of \mathbf{U} represent an optimized subspace of order p (in the mean square sense) for \mathbb{F} and can be seen as a point on the Grassmann manifold $\mathcal{G}(p, d)$.

Modeling by linear subspaces generally does not take into account the order of images. While this property sounds restrictive, in many practical situations (like object recognition from video), the order of frames may not be important for decision making. However, it is possible to capture information related to order through an extended type of image-sets, obtained through a block Hankel matrix formalism (Li et al. 2011).

7.1.2 Modeling of Dynamics

A video can be represented by an ARMA model to explicitly capture dynamics (Doretto et al. 2003; Turaga et al. 2011). A set of ordered images $\{\mathbf{f}(t)\}_{t=1}^\tau; \mathbf{f}(t) \in \mathbb{R}^d$ can be modeled as the output of an ARMA model by:

$$\mathbf{x}(t) = \mathbf{C}\mathbf{z}(t) + \mathbf{w}(t), \quad \mathbf{w}(t) \sim \mathcal{N}(0, \mathbf{R}) \quad (34)$$

$$\mathbf{z}(t+1) = \mathbf{A}\mathbf{z}(t) + \mathbf{v}(t), \quad \mathbf{v}(t) \sim \mathcal{N}(0, \mathbf{Q}) \quad (35)$$

where $\mathbf{z}(t) \in \mathbb{R}^n$ is the hidden state vector at time t , $\mathbf{A} \in \mathbb{R}^{n \times n}$ and $\mathbf{C} \in \mathbb{R}^{d \times n}$ are the transition and measurement matrices, respectively, while \mathbf{w} and \mathbf{v} are noise components modeled as normal distributions with zero mean and covariance matrices $\mathbf{R} \in \mathbb{R}^{d \times d}$ and $\mathbf{Q} \in \mathbb{R}^{n \times n}$, respectively. Loosely speaking, one advantage of the ARMA model is that it decouples the appearance of the spatio-temporal data (modeled by \mathbf{C}) from the dynamics (represented by \mathbf{A}).

The transition and measurement matrices can be estimated through a set of feature vectors. More specifically, if $\mathbb{F}_\tau = [\mathbf{f}(1)|\mathbf{f}(2)|\dots|\mathbf{f}(\tau)]$ represents the feature matrix for time indexes $1, 2, \dots, \tau$, the estimated transition $\hat{\mathbf{A}}$ and measurement $\hat{\mathbf{C}}$ matrices can be obtained via the SVD of $\mathbb{F}_\tau = \mathbf{U}\mathbf{\Sigma}\mathbf{V}^T$, as follows:

$$\hat{\mathbf{A}} = \mathbf{\Sigma}\mathbf{V}^T\mathbf{D}_1\mathbf{V}(\mathbf{V}^T\mathbf{D}_2\mathbf{V})^{-1}\mathbf{\Sigma}^{-1}. \quad (36)$$

$$\hat{\mathbf{C}} = \mathbf{U}. \quad (37)$$

where

$$\mathbf{D}_1 = \begin{bmatrix} \mathbf{0}_{\tau-1}^T & 0 \\ \mathbf{I}_{(\tau-1) \times (\tau-1)} & \mathbf{0}_{\tau-1} \end{bmatrix} \quad \text{and} \quad \mathbf{D}_2 = \begin{bmatrix} \mathbf{I}_{(\tau-1) \times (\tau-1)} & \mathbf{0}_{\tau-1} \\ \mathbf{0}_{\tau-1}^T & 0 \end{bmatrix}.$$

Two ARMA models can be compared based on the subspace angles between the column-spaces of their observability matrices (Cock and Moor 2002). The extended observability matrix of an ARMA model is given by

$$\mathbf{O}_\infty = [\mathbf{C}^T | (\mathbf{C}\mathbf{A})^T | (\mathbf{C}\mathbf{A}^2)^T | \dots | (\mathbf{C}\mathbf{A}^n)^T | \dots]^T .$$

The extended observability matrix is usually approximated by the finite observability matrix as (Turaga et al. 2011):

$$\mathbf{O}_m = \left[\hat{\mathbf{C}}^T | (\hat{\mathbf{C}}\hat{\mathbf{A}})^T | (\hat{\mathbf{C}}\hat{\mathbf{A}}^2)^T | \dots | (\hat{\mathbf{C}}\hat{\mathbf{A}}^{(m-1)})^T \right]^T . \quad (38)$$

For a given video, the finite observability parameter of the ARMA model is estimated as described above. To represent the subspace spanned by the columns of \mathbf{O}_m , an orthonormal basis can be computed through Gram-Schmidt orthonormalization. As a result, a dynamic linear system can be described as a point on a Grassmann manifold corresponding to the column space of the observability matrix. We note that appearance modeling presented in § 7.1.1 can be seen as a special case of ARMA modeling, where $m = 1$.

7.2 Coding on Grassmann Manifolds

In this part we compare and contrast the performance of the proposed methods against several state-of-the-art methods: Discriminant Canonical Correlation Analysis (DCCA) (Kim et al. 2007), kernelized Affine Hull Method (KAHM) (Cevikalp and Triggs 2010), Grassmann Discriminant Analysis (GDA) (Hamm and Lee 2008), and Graph-embedding Grassmann Discriminant Analysis (GGDA) (Harandi et al. 2011). We evaluate the performance on the tasks of (i) gender recognition from gait, (ii) hand gesture recognition, and (iii) scene analysis.

DCCA is an iterative learning method that maximizes a measure of discrimination between image sets where the distance between sets is expressed by canonical correlations. In KAHM, images are considered as points in a linear or affine feature space, while image sets are characterized by a convex geometric region (affine or convex hull) spanned by their feature points. GDA can be considered as an extension of kernel discriminant analysis over Grassmann manifolds (Hamm and Lee 2008). In GDA, a transform over the Grassmann manifold is learned to simultaneously maximize a measure of inter-class distances and minimize intra-class distances. GGDA can be considered as an extension of GDA, where a local discriminant transform over Grassmann manifolds is learned. This is achieved by incorporating local similarities/dissimilarities through within-class and between-class similarity graphs.

We denote Grassmann sparse coding, Grassmann locality linear coding and their kernel extensions by *gSC*, *gLLC*, *kgSC* and *kgLLC*, respectively. Based on preliminary experiments, the Gaussian kernel (Shawe-Taylor and Cristianini 2004), defined as $k(\mathbf{a}, \mathbf{b}) = \exp(-\gamma\|\mathbf{a} - \mathbf{b}\|^2)$, was used in kgSC and kgLLC. The value of the γ parameter in all experiments was determined by cross validation.

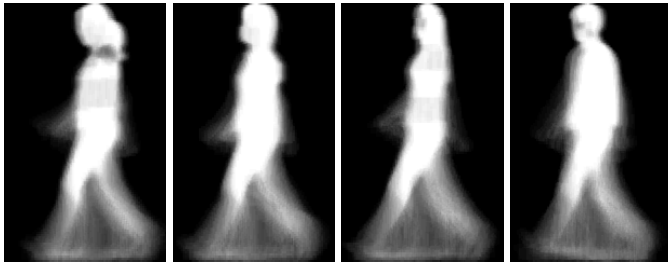


Fig. 4: GEI samples from the CASIA gait dataset (Zheng et al. 2011).

Table 1: Recognition rate on the CASIA dataset for KAHM (Cevikalp and Triggs 2010), GDA (Hamm and Lee 2008), GGDA (Harandi et al. 2011) and the proposed approaches.

Method	Accuracy
DCCA (Kim et al. 2007)	85.9 ± 6.6
KAHM (Cevikalp and Triggs 2010)	89.8 ± 2.4
GDA (Hamm and Lee 2008)	76.4 ± 5.8
GGDA (Harandi et al. 2011)	84.3 ± 4.8
gSC	94.3 ± 2.1
gLLC	93.7 ± 2.1
kgSC	95.6 ± 2.1
kgLLC	95.2 ± 1.6

7.2.1 Gender Recognition from Gait

Gait is defined as “manner of walking” and can be used as a biometric measure to recognize, among other things, the gender of humans (Yu et al. 2009b). For the task of gender recognition from gait data, we have used Dataset-B of the CASIA Gait Database (Zheng et al. 2011) which constitutes of 124 individuals (93 males and 31 females). In the CASIA dataset, the gait of each subject has been captured from 11 angles. Every video is represented by one gait energy image (GEI) of size 32×32 , which has been shown to be effective in recognition of gender (Yu et al. 2009b). Cropped samples of GEI images are shown in Fig. 4.

We used the videos captured with normal clothes and created a subspace of order 6 (based on preliminary experiments) using the corresponding 11 GEIs. This resulted in 731 points on $\mathcal{G}_{1024,6}$. We then randomly selected 20 individuals (10 male, 10 female) as the training set and used the remaining individuals for testing. There is no overlap of individuals between the training and test sets.

Table 1 shows a comparison of gSC, gLLC and their kernelized versions against DCCA, KAHM, GDA and GGDA. All four proposed methods consistently outperform previous state-of-the-art algorithms with a big margin. The highest accuracy is attained by kgSC, followed by kgLLC. As expected, the kernel extensions perform better than gSC and gLLC. However, the burden of determining the kernel parameters sometimes could be overwhelming.

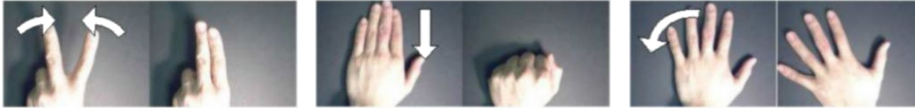


Fig. 5: Examples of hand actions in the Cambridge dataset (Kim and Cipolla 2009).

7.2.2 Hand Gesture Recognition

For the hand-gesture recognition task, we used the Cambridge hand-gesture dataset (Kim and Cipolla 2009) which consists of 900 image sequences of 9 gesture classes. Each class has 100 image sequences performed by 2 subjects, captured under 5 illuminations and 10 arbitrary motions. The 9 classes are defined by three primitive hand shapes and three primitive motions. Each sequence was recorded at 30 fps with a resolution of 320×240 , in front of a fixed camera having roughly isolated gestures in space and time. See Fig. 5 for examples. We followed the test protocol defined by Kim and Cipolla (2009), and resized all sequences to $20 \times 20 \times 20$. Sequences with normal illumination are considered for training while the remaining sequences (with different illumination characteristics) are used for testing.

As per Kim and Cipolla (2009), we report the recognition rates for the four illumination sets. In addition to GDA, GGDA and KAHM, the proposed methods were also compared against Tensor Canonical Correlation Analysis (TCCA) (Kim and Cipolla 2009) and Product Manifolds (PM) (Lui 2012). TCCA, as the name implies, is the extension of canonical correlation analysis to multiway data arrays or tensors. Canonical correlation analysis is a standard method for measuring the similarity between subspaces (Kim and Cipolla 2009). In the PM method a tensor is characterized as a point on a product manifold and classification is performed on this space. The product manifold is created by applying a modified high order singular value decomposition on the tensors and interpreting each factorized space as a Grassmann manifold.

For Grassmann-based methods, we represented each video through ARMA modeling. The observability order of the ARMA model (m in Eqn. (38)) and the subspace dimension (order of matrix C) were selected as 5 and 10, respectively. The results, presented in Table 2, show that the proposed approaches obtain the highest performance. kgLLC achieves the best recognition accuracy on all four sets. KAHM performs very poorly in this task, which we conjecture is due to the illumination differences between the training and test sets.

7.3 Scene Analysis

For scene analysis, we employed the UCSD traffic dataset (Chan and Vasconcelos 2005), which contains 254 video sequences of highway traffic of varying patterns (*e.g.* light, heavy) in various weather conditions (*e.g.*, cloudy, raining, sunny). Each video was recorded with a resolution of 320×240 pixels, for a duration ranging from 42 to 52 frames. Here we have used a normalized grayscale 48×48 version of the dataset. The normalization process for each video clip involves subtracting the mean image and normalizing the pixel intensities to unit variance. This is useful to reduce the impact of illumination variations.

Method	Set1	Set2	Set3	Set4	Overall
TCCA (Kim and Cipolla 2009)	81	81	78	86	82 ± 3.5
KAHM (Cevikalp and Triggs 2010)	43	43	43	41	43 ± 1.4
GDA (Hamm and Lee 2008)	92	85	84	87	87.4 ± 3.8
GGDA (Harandi et al. 2011)	91	91	88	94	91.1 ± 2.5
PM (Lui 2012)	93	89	91	94	91.7 ± 2.3
gSC	93	92	93	94	93.3 ± 0.9
gLLC	96	94	96	97	95.4 ± 1.3
kgSC	96	92	93	97	94.4 ± 2.0
kgLLC	96	94	96	98	95.7 ± 1.6

Table 2: **Hand-gesture recognition.** Recognition accuracy for the hand-gesture recognition task using KAHM (Cevikalp and Triggs 2010), GDA (Hamm and Lee 2008), GGDA (Harandi et al. 2011), TCCA (Kim and Cipolla 2009), Product Manifold (PM) (Lui 2012) and the proposed approaches.



Fig. 6: Representative examples of the three classes in UCSD traffic video dataset (Chan and Vasconcelos 2005). From left to right: examples of light, medium, and heavy traffic.

The dataset is labeled into three classes with respect to the amount of traffic congestion in each sequence. In total there are 44 sequences of heavy traffic (slow or stop-and-go speeds), 45 of medium traffic (reduced speed), and 165 of light traffic (normal speed). See Fig. 6 for examples.

We represented each video on a Grassmann manifold through ARMA modeling. The observability order of the ARMA model and the subspace dimension were selected as 5 and 10 respectively.

In addition to GDA, GGDA and KAHM, the proposed methods were also compared against Linear Dynamical System (LDS) and Compressive Sensing Linear Dynamical System (CS-LDS) (Sankaranarayanan et al. 2010). The results, presented in Table 3, show that the proposed approaches obtain the best overall performance, with kgLLC achieving the highest overall accuracy.

7.4 Dictionary Learning

Here we analyze the performance of the proposed dictionary learning techniques as described in § 6 on three classification tasks: face recognition, action recognition and dynamic texture classification. In all the following experiments, an SVM classifier with a Gaussian kernel was used to perform recognition. That is, the training and testing data were first coded by the learned dictionary and then the sparse codes were fed to an SVM classifier. Parameters for the SVM classifier were determined by cross validation.

Table 3: Average correct recognition rate on the UCSD video traffic dataset for dynamic spatio-temporal models using LDS (Sankaranarayanan et al. 2010), Compressive-Sensing LDS (Sankaranarayanan et al. 2010), GDA (Hamm and Lee 2008), GGDA (Harandi et al. 2011), and the proposed approaches.

Method	Exp1	Exp2	Exp3	Exp4	Overall
LDS (Sankaranarayanan et al. 2010)	85.7	85.9	87.5	92.1	87.8 \pm 3.0
CS-LDS (Sankaranarayanan et al. 2010)	84.1	87.5	89.1	85.7	86.6 \pm 2.2
KAHM (Cevikalp and Triggs 2010)	84.1	79.7	82.8	84.1	82.7 \pm 2.1
GDA (Hamm and Lee 2008)	82.5	85.9	70.3	77.8	79.1 \pm 6.7
GGDA (Harandi et al. 2011)	87.3	89.1	90.6	90.5	89.4 \pm 1.5
gSC	93.7	87.5	95.3	95.2	92.9 \pm 3.7
gLLC	96.8	85.9	92.2	93.7	92.2 \pm 4.5
kgSC	96.8	89.1	95.3	98.4	94.9 \pm 4.1
kgLLC	95.2	92.2	96.9	96.8	95.3 \pm 2.2

7.4.1 Face Recognition

While face recognition from a single still image has been extensively studied, recognition based on a group of still images is relatively new. A popular choice for modeling image-sets is by representing them through linear subspaces (Hamm and Lee 2008; Harandi et al. 2011). For the task of image-set face recognition, we used the YouTube celebrity dataset (Kim et al. 2008) which contains 1910 video clips of 47 subjects. See Fig. 7 for examples. Face recognition on this dataset is challenging, since the videos have a high compression ratio and most of them are low-resolution.

To create an image set from a video, we used a cascaded face locator (Viola and Jones 2004) to extract face regions from each video, followed by resizing regions to 96×96 and describing them via histogram of Local Binary Patterns (LBP) (Ojala et al. 2002). Then each image set (corresponding to a video) was represented by a linear subspace of order 5. We randomly chose 70% of the dataset for training and the remaining 30% for testing. The process of random splitting was repeated ten times and the average classification accuracy is reported.

The results in Table 4 show that the proposed coding methods (using dictionaries provided by their corresponding dictionary learning algorithms) outperform the competitors. kgSC with dictionary learning achieved the highest accuracy of 73.91, more than 3 percentage points better than gSC with dictionary learning. Similarly, the performance of kgLLC with dictionary learning is observed to be higher than gLLC with dictionary learning.

7.4.2 Ballet Dataset

The Ballet dataset contains 44 videos collected from an instructional ballet DVD (Wang and Mori 2009). The dataset consists of 8 complex motion patterns performed by 3 subjects. The actions include: ‘left-to-right hand opening’, ‘right-to-left hand opening’, ‘standing hand opening’, ‘leg swinging’, ‘jumping’, ‘turning’, ‘hopping’ and ‘standing still’. Fig. 8 shows examples. The dataset is challenging due to the significant intra-class variations in terms of speed, spatial and temporal scale, clothing and movement.



Fig. 7: Examples of YouTube celebrity dataset (grayscale versions of images were used in our experiments).

We extracted 2400 image sets by grouping 6 frames that exhibited the same action into one image set. We described each image set by a subspace of order 4 with Histogram of Oriented Gradient (HOG) as frame descriptor (Dalal and Triggs 2005). Available samples were randomly split into training and testing sets (the number of image sets in both sets was even). The process of random splitting was repeated ten times and the average classification accuracy is reported⁴.

Table 5 shows that all proposed coding approaches have superior performance as compared to DCC, KAHM, GDA and GGDA. For example, the difference between gSC with dictionary learning (gSC-dic) and the closest state-of-the-art competitor (GGDA), is more than six percentage points.

7.4.3 Dynamic Texture Classification

Dynamic textures are videos of moving scenes that exhibit certain stationary properties in the time domain (Ghanem and Ahuja 2010; Xu et al. 2011). Such videos

⁴ Wang and Mori (2009) addressed the problem of recognizing actions in still images. This is different from the work presented here, where we focus on recognition using videos and image sets.

Table 4: Average recognition rate on the YouTube celebrity dataset.

Method	CRR
DCC (Kim et al. 2007)	60.21 ± 2.9
KAHM (Cevikalp and Triggs 2010)	67.49 ± 3.5
GDA (Hamm and Lee 2008)	58.72 ± 3.0
GGDA (Harandi et al. 2011)	61.06 ± 2.2
gSC-dic	70.47 ± 1.7
gLLC-dic	71.74 ± 2.3
kgSC-dic	73.91 ± 1.9
kgLLC-dic	73.53 ± 2.3



Fig. 8: Examples from the Ballet dataset (Wang and Mori 2009).

are pervasive in various environments, such as sequences of rivers, clouds, fire, swarms of birds, humans in crowds. In our experiment, we used the challenging DynTex++ dataset (Ghanem and Ahuja 2010), which is comprised of 36 classes, each of which contains 100 sequences with a fixed size of $50 \times 50 \times 50$ (see Fig. 9 for example classes). We split the dataset into training and testing sets by randomly assigning half of the videos of each class to the training set and using the rest as query data. The random split was repeated twenty times; average accuracy is reported.

To generate Grassmann points, we used histogram of LBP from Three Orthogonal Planes (LBP-TOP) (Zhao and Pietikainen 2007) which takes into account the dynamics within the videos. To this end, each video is split into subvideos of length 10, with a 7 frame overlap. Each subvideo is then described by a histogram of LBP-TOP features. From the subvideo descriptors, we extracted a subspace of order 5 as the video representation on a Grassmann manifold.

In addition to DCC, KAHM, GDA and GGDA, the proposed approaches were compared against two methods specifically designed for dynamic texture classification: dynamic fractal spectrum (DFS) (Xu et al. 2011) and Distance Learning Pegasos (DL-Pegasos) (Ghanem and Ahuja 2010). DFS can be seen as concatenation of two components: (i) a volumetric component that encodes the stochas-

Table 5: Average recognition rate on the Ballet dataset.

Method	CRR
DCC (Kim et al. 2007)	41.95 \pm 9.6
KAHM (Cevikalp and Triggs 2010)	70.05 \pm 0.9
GDA (Hamm and Lee 2008)	67.33 \pm 1.1
GGDA (Harandi et al. 2011)	73.54 \pm 2.0
gSC-dic	79.64 \pm 1.1
gLLC-dic	81.42 \pm 0.8
kgSC-dic	83.53 \pm 0.8
kgLLC-dic	86.94 \pm 1.1



Fig. 9: Example classes of DynTex++ dataset (grayscale images were used in our experiments).

Table 6: Average recognition rate on the DynTex++ dataset.

Method	CRR
DL-PEGASOS (Ghanem and Ahuja 2010)	63.7
DFS (Xu et al. 2011)	89.9
DCC (Kim et al. 2007)	53.2
KAHM (Cevikalp and Triggs 2010)	82.8
GDA (Hamm and Lee 2008)	81.2
GGDA (Harandi et al. 2011)	84.1
gSC-dic	90.3
gLLC-dic	91.8
kgSC-dic	92.8
kgLLC-dic	93.2

tic self-similarities of dynamic textures as 3D volumes, (ii) a multi-slice dynamic component that captures structures of dynamic textures on 2D slices along various views of the 3D volume. DL-Pegasos uses three descriptors (LBP, HOG and LDS) and learns how the descriptors can be linearly combined to best discriminate between dynamic texture classes.

The overall classification results are presented in Table 6. The proposed kgLLC with dictionary learning (kgLLC-dic) obtains the highest average recognition rate.

8 Further Discussion

A seemingly straightforward method for obtaining sparse codes is through embedding manifolds into Euclidean spaces via tangent spaces. The embedding function in this case would be $\log_{\mathbf{P}}(\cdot)$, where \mathbf{P} is the center of projection. The natural choice for the center of projection in the literature is

$$\mathbf{P} = \begin{bmatrix} \mathbf{I}_{p \times p} \\ \mathbf{0}_{(n-p) \times p} \end{bmatrix}.$$

By embedding Grassmann points on the tangent space, the sparse representation problem is transformed to its Euclidean counterpart. We illustrate the corresponding steps in Algorithm 7. We shall refer to this straightforward approach as

Algorithm 7: Log-Euclidean sparse coding on Grassmann manifolds.**Input:** Grassmann dictionary $\{\mathbf{D}_i\}_{i=1}^N$, $\mathbf{D}_i \in \mathcal{G}(p, d)$; the query sample $\mathbf{X} \in \mathcal{G}(p, d)$.**Output:** The sparse code \mathbf{y}^* .**Initialization.**

```

for  $i \leftarrow 1$  to  $N$  do
  |  $\mathbf{d}_i \leftarrow \log_{\mathcal{P}}(\mathbf{D}_i)$ ;
end
 $\mathbf{A} \leftarrow [\mathbf{d}_1 | \mathbf{d}_2 | \dots | \mathbf{d}_N]$ ;

```

Processing.

```

 $\mathbf{x} \leftarrow \log_{\mathcal{P}}(\mathbf{X})$ ;
 $\mathbf{y}^* \leftarrow \arg \min_{\mathbf{y}} \|\mathbf{x} - \mathbf{A}\mathbf{y}^T\|_2^2 + \lambda \|\mathbf{y}\|_1$ ;

```

Log-Euclidean sparse coding, following the terminology used in differential geometry (Arsigny *et al.* 2006). Since on a tangent space only distances to the center of projection are equal to true geodesic distances, Log-Euclidean solution does not take into account the true structure of the underlying Riemannian manifold.

A more elegant way of performing sparse coding on Riemannian manifolds has been recently proposed by Ho *et al.* (2013). The idea is to consider the tangent space of a query point \mathbf{X} to perform sparse coding. This guarantees that the true geodesic distances are considered in sparse coding. However, since $\log_{\mathbf{X}}(\mathbf{X}) = \mathbf{0}$, the sparse coding has the trivial solution $\mathbf{0}$. Through the notion of invariance in origin (Ho *et al.* 2013), this degeneracy can be avoided by having an extra constraint similar to LLC. More specifically, let $\mathbf{d}_{\mathbf{X},j} = \log_{\mathbf{X}}(\mathbf{D}_j)$ be the vector representation of \mathbf{D}_j to the tangent space of the query point \mathbf{X} . Then the intrinsic sparse codes are obtained as the solution of:

$$\min_{\mathbf{y}} \left\| \sum_{j=1}^N [\mathbf{y}]_j \mathbf{d}_{\mathbf{X},j} \right\|^2 \quad (39)$$

s.t. $\mathbf{1}^T \mathbf{y} = 1$.

To contrast the Log-Euclidean (IE-SC) and intrinsic (iSC) (Ho *et al.* 2013) solutions against the proposed gSC approach we performed two experiments with synthetic data. Specifically, we considered two multi-class classification problems over $\mathcal{G}(2, 6)$. The first experiment involved a relatively simple classification problem that matched the properties of the Log-Euclidean approach, while the second experiment considered a more realistic scenario.

In both experiments, we randomly generated four classes over the $\mathcal{G}(2, 6)$, where the samples in each class obey a normal distribution on a specific tangent space of $\mathcal{G}(2, 6)$. This can be achieved by considering normal distributions over the specific tangent space of $\mathcal{G}(2, 6)$ followed by mapping the points back to $\mathcal{G}(2, 6)$ using the exponential map (see Algorithm 9 for details of the exponential map). We created four classification problems with increasing difficulty, by fixing the mean of each class and increasing the class variance. In the following discussion, the problems will be referred as ‘easy’, ‘medium’, ‘hard’, and ‘very hard’.

For a given problem, 8 samples per class were considered as the dictionary atoms, while 1000 samples per class were generated as query data. This results

Table 7: Comparison of the proposed gSC approach with the Log-Euclidean sparse coding (lE-SC) and intrinsic sparse coding (iSC) (Ho et al. 2013) methods on synthetic data. In the first experiment, samples in each class obey a normal distribution over the identity tangent space. The second experiment reflects a more challenging scenario where samples in each class obey a normal distribution over a random tangent space, instead of the identity tangent space.

Task	Experiment #1		Experiment #2	
	Easy	Medium	Hard	Very Hard
lE-SC	99.5%	90.8%	55.7%	49.9%
iSC (Ho et al. 2013)	98.6%	84.1%	64.7%	53.4%
gSC	99.2%	86.6%	66.9%	57.4%

in a multiclass recognition problem with 4000 samples and a dictionary of size 32. All the generated samples were then mapped back to the manifold using the exponential map and were duly used in the Log-Euclidean, intrinsic and the proposed sparse coding approaches. For each task, the data generation procedure was repeated ten times; average recognition rates are reported.

In the first experiment, we considered distributions over the identity tangent space, *i.e.*, $\mathbf{P} = \begin{bmatrix} \mathbf{I}_{2 \times 2} \\ \mathbf{0} \end{bmatrix}$. The results are presented in Table 7 under Experiment #1. By increasing the class variance, samples from various classes are intertwined, which in turn leads to a decrease in recognition accuracy. Even though this experiment matches the characteristics of the Log-Euclidean approach (since the prior knowledge of class distribution is available), both gSC and iSC approaches obtain on par performance for the easy case. For the medium case, Log-Euclidean approach achieves the highest accuracy followed by gSC and iSC.

In the second experiment we relaxed the location of tangent space in order to simulate a more challenging scenario. More specifically, instead of generating distributions over the identity tangent space, the tangent space was selected randomly. As shown in Table 7 under Experiment #2, the Log-Euclidean approach performs poorly when compared to gSC and iSC. The gSC approach consistently outperforms iSC, which we conjecture might be due to the extra constraint in iSC (the affine constraint).

We also performed an additional experiment to measure the approximate computational complexities of gSC and iSC. Assuming that the complexity of vector sparse coding for both algorithms is similar (iSC is a constrained coding approach so it is very likely to be more expensive than an unconstrained one like gSC), we measured the time required to prepare the data for both algorithms. More specifically, for a query point $\mathbf{X} \in \mathcal{G}(p, d)$, gSC requires the vector $\mathcal{K}_{\mathbf{X}}$ as defined in Eq. (11). For iSC, all dictionary atoms must be projected to the tangent space of \mathbf{X} . To measure the complexity of the aforementioned processes (computing $\mathcal{K}_{\mathbf{X}}$ and projecting \mathbb{D} to the tangent space of \mathbf{X}), we considered three cases using the geometry of $\mathcal{G}(3, 10)$, $\mathcal{G}(3, 100)$ and $\mathcal{G}(3, 1000)$. We randomly generated a dictionary of size 1000 for each case (*i.e.*, $\mathcal{G}(3, 10)$, $\mathcal{G}(3, 100)$ and $\mathcal{G}(3, 1000)$) and measured the time required to compute $\mathcal{K}_{\mathbf{X}}$ and tangent projection for 1000 query points.

The results are given in Table 8. The gSC algorithm is several orders of magnitude faster than iSC, especially for high-dimensional subspaces. We note that iSC is even more demanding when it comes to dictionary learning as the algorithm requires switching back and forth to tangent spaces of manifolds.

Table 8: Running time comparison between the proposed gSC approach and intrinsic sparse coding (iSC) (Ho et al. 2013) method on synthetic data. Times are measured in second on a Quad-core i7 machine with Matlab.

Task	$\mathcal{G}(3, 10)$	$\mathcal{G}(3, 100)$	$\mathcal{G}(3, 1000)$
iSC (Ho et al. 2013)	383.8s	662.2s	22490.3s
gSC	3.1s	4.1s	32.5s

9 Main Findings and Future Directions

With the aim of coding on Grassmann manifolds, we proposed to embed such manifolds into the space of symmetric matrices by an isometric projection. We then showed how sparse coding and locality linear coding can be performed in the induced space. We also tackled the problem of dictionary learning on Grassmann manifolds and devised a closed-form solution for updating a dictionary atom by atom, using the geometry of induced space. Finally, we proposed a kernelized version of sparse coding, locality linear coding and dictionary learning on Grassmann manifolds, to handle non-linearity in data.

Experiments on several classification tasks (gender recognition, gesture classification, scene analysis, face recognition, action recognition and dynamic texture classification) show that the proposed approaches achieve notable improvements in discrimination accuracy, in comparison to state-of-the-art methods such as discriminant analysis of canonical correlation analysis (Kim et al. 2007) affine hull method (Cevikalp and Triggs 2010), Grassmann discriminant analysis (Hamm and Lee 2008), and graph-embedding Grassmann discriminant analysis (Harandi et al. 2011).

In this work a Grassmann dictionary is learned such that a reconstruction error is minimized. This is not necessarily the optimum solution when labeled data is available. To benefit from labeled data, it has recently been proposed to consider a discriminative penalty term along with the reconstruction error term in the optimization process (Mairal et al. 2012). We are currently pursuing this line of research and seeking solutions for discriminative dictionary learning on Grassmann manifolds. Moreover, our formulation can be understood as an extrinsic solution to the problem of coding and dictionary learning on Grassmann manifolds. It would be interesting to devise intrinsic solutions based on the geometry of the induced space, *i.e.*, symmetric matrices.

Appendices

A Proofs

Here, we prove Theorems 2 and 3 from § 3.1. For readability purposes, we repeat the theorems before the proofs.

Theorem 2 (Length Equivalency) *The length of any given curve is the same under δ_s and δ_g up to a scale of $\sqrt{2}$.*

Proof Proof of this theorem is developed in several steps. We start with the definition of curve length and intrinsic metric. Without any assumption on differentiability, let (M, d) be a metric space. A curve in M is a continuous function $\gamma : [0, 1] \rightarrow M$ and joins the starting point $\gamma(0) = x$ to the end point $\gamma(1) = y$. With slight abuse of notation L , let us define the following:

Definition 5 The length of a curve γ is the supremum of $L(\gamma; \{t_i\})$ over all possible partitions $\{t_i\}$ with $\{t_i\}$ being $0 = t_0 < t_1 < \dots < t_{n-1} < t_n = 1$ and $L(\gamma; \{t_i\}) = \sum_i d(\gamma(t_i), \gamma(t_{i-1}))$.

Definition 6 The intrinsic metric $\widehat{\delta}$ is defined as the infimum of the lengths of all paths from x to y .

Theorem 5 If the intrinsic metrics induced by two metrics d_1 and d_2 are identical to scale ξ , then the length of any given curve is the same under both metrics up to ξ .

Proof We refer the reader to (Hartley et al. 2013) for the proof of this theorem. \square

Theorem 6 If $d_1(x, y)$ and $d_2(x, y)$ are two metrics defined on a space M such that

$$\lim_{d_1(x, y) \rightarrow 0} \frac{d_2(x, y)}{d_1(x, y)} = 1. \quad (40)$$

uniformly (with respect to x and y), then their intrinsic metrics are identical.

Proof We refer the reader to (Hartley et al. 2013) for the proof of this theorem. \square

Therefore, we need to study the behavior of

$$\lim_{\delta_g(\mathbf{X}, \mathbf{Y}) \rightarrow 0} \frac{\delta_s(\mathbf{X}, \mathbf{Y})}{\delta_g(\mathbf{X}, \mathbf{Y})},$$

to prove our theorem on curve lengths. We note that

$$\delta_s^2(\mathbf{X}, \mathbf{Y}) = \|\mathbf{X}\mathbf{X}^T - \mathbf{Y}\mathbf{Y}^T\|_F^2 = 2 \sum_{i=1}^p \sin^2 \theta_i.$$

Since $\sin \theta_i \rightarrow \theta_i$ for $\theta_i \rightarrow 0$, it can be seen that

$$\lim_{\delta_g(\mathbf{X}, \mathbf{Y}) \rightarrow 0} \frac{\delta_s^2(\mathbf{X}, \mathbf{Y})}{\delta_g^2(\mathbf{X}, \mathbf{Y})} = \lim_{\delta_g(\mathbf{X}, \mathbf{Y}) \rightarrow 0} \frac{2 \sum_{i=1}^p \sin^2 \theta_i}{\sum_{i=1}^p \theta_i^2} = 2,$$

which concludes the proof. \square

Theorem 3 (Closed-Form Mean) The Karcher mean for a set of points $\{\mathbf{X}_i\}_{i=1}^N$, $\mathbf{X}_i \in \mathcal{G}(p, d)$ in the embedded space, defined as

$$\begin{aligned} \mathbf{X}^* &\triangleq \arg \min_{\mathbf{X}} \sum_{i=1}^N \left\| \mathbf{X}\mathbf{X}^T - \mathbf{X}_i\mathbf{X}_i^T \right\|_F^2, \\ \text{s.t. } &\mathbf{X}^T \mathbf{X} = \mathbf{I}_p, \end{aligned} \quad (41)$$

admits a closed-form solution.

Proof We note that

$$\begin{aligned} \sum_{i=1}^N \left\| \mathbf{X}\mathbf{X}^T - \mathbf{X}_i\mathbf{X}_i^T \right\|_F^2 &= 2pN - \sum_{i=1}^N \text{Tr}\{\mathbf{X}^T \mathbf{X}_i \mathbf{X}_i^T \mathbf{X}\} \\ &= 2pN - \text{Tr}\left\{ \mathbf{X}^T \left(\sum_{i=1}^N \mathbf{X}_i \mathbf{X}_i^T \right) \mathbf{X} \right\}. \end{aligned}$$

Therefore to minimize Eq. (41), one should maximize $\text{Tr}\{\mathbf{X}^T \left(\sum_{i=1}^N \mathbf{X}_i \mathbf{X}_i^T \right) \mathbf{X}\}$ by taking into account the constraint $\mathbf{X}^T \mathbf{X} = \mathbf{I}_p$, *i.e.*,

$$\mathbf{X}^* \triangleq \arg \max_{\mathbf{X}} \text{Tr}\{\mathbf{X}^T \left(\sum_{i=1}^N \mathbf{X}_i \mathbf{X}_i^T \right) \mathbf{X}\}, \quad (42)$$

$$\text{s.t. } \mathbf{X}^T \mathbf{X} = \mathbf{I}_p.$$

The solution of Eq. (42) is obtained by computing the p largest eigenvectors of $\sum_{i=1}^N \mathbf{X}_i \mathbf{X}_i^T$ according to the Rayleigh-Ritz theorem (Horn and Johnson 2012), which concludes the proof. \square

Theorem 4 *The geometric mean of \mathbf{X} and \mathbf{Y} coincides with its Karcher mean in the embedded projection space.*

Proof The geometric mean of \mathbf{X} and \mathbf{Y} on the $\mathcal{G}(p, d)$, *i.e.*, $\mathbf{X} \# \mathbf{Y}$ is given by Eq. (9). We first show that columns of $\mathbf{X} \# \mathbf{Y}$ are eigenvectors of $\mathbf{X} \mathbf{X}^T + \mathbf{Y} \mathbf{Y}^T$. Since $\mathbf{X} \mathbf{X}^T + \mathbf{Y} \mathbf{Y}^T$ is symmetric, its eigenvectors are orthogonal. Therefore, we need to show that $(\mathbf{X} \# \mathbf{Y})^T (\mathbf{X} \mathbf{X}^T + \mathbf{Y} \mathbf{Y}^T) \mathbf{X} \# \mathbf{Y}$ is a diagonal matrix with the eigenvalues being the elements of the resulting diagonal matrix.

$$\begin{aligned} & (\mathbf{X} \# \mathbf{Y})^T (\mathbf{X} \mathbf{X}^T + \mathbf{Y} \mathbf{Y}^T) \mathbf{X} \# \mathbf{Y} \\ &= \left(\mathbf{X} \mathbf{U}_1 \Gamma \left(\frac{1}{2} \right) - \mathbf{X}_\perp \mathbf{U}_2 \Sigma \left(\frac{1}{2} \right) \right)^T (\mathbf{X} \mathbf{X}^T + \mathbf{Y} \mathbf{Y}^T) \left(\mathbf{X} \mathbf{U}_1 \Gamma \left(\frac{1}{2} \right) - \mathbf{X}_\perp \mathbf{U}_2 \Sigma \left(\frac{1}{2} \right) \right) \\ &= \left(\Gamma \left(\frac{1}{2} \right) \mathbf{U}_1^T \mathbf{X}^T + \Gamma \left(\frac{1}{2} \right) \mathbf{U}_1^T \mathbf{X}^T \mathbf{Y} \mathbf{Y}^T - \Sigma \left(\frac{1}{2} \right) \mathbf{U}_2^T \mathbf{X}_\perp^T \mathbf{Y} \mathbf{Y}^T \right) \left(\mathbf{X} \mathbf{U}_1 \Gamma \left(\frac{1}{2} \right) - \mathbf{X}_\perp \mathbf{U}_2 \Sigma \left(\frac{1}{2} \right) \right) \\ &= \Gamma \left(\frac{1}{2} \right) \mathbf{U}_1^T \mathbf{U}_1 \Gamma \left(\frac{1}{2} \right) + \Gamma \left(\frac{1}{2} \right) \mathbf{U}_1^T \mathbf{X}^T \mathbf{Y} \mathbf{Y}^T \mathbf{X} \mathbf{U}_1 \Gamma \left(\frac{1}{2} \right) - \Sigma \left(\frac{1}{2} \right) \mathbf{U}_2^T \mathbf{X}_\perp^T \mathbf{Y} \mathbf{Y}^T \mathbf{X} \mathbf{U}_1 \Gamma \left(\frac{1}{2} \right) \\ &\quad - \Gamma \left(\frac{1}{2} \right) \mathbf{U}_1^T \mathbf{X}^T \mathbf{Y} \mathbf{Y}^T \mathbf{X}_\perp \mathbf{U}_2 \Sigma \left(\frac{1}{2} \right) + \Sigma \left(\frac{1}{2} \right) \mathbf{U}_2^T \mathbf{X}_\perp^T \mathbf{Y} \mathbf{Y}^T \mathbf{X}_\perp \mathbf{U}_2 \Sigma \left(\frac{1}{2} \right) \\ &= \Gamma^2 \left(\frac{1}{2} \right) + \Gamma \left(\frac{1}{2} \right) \mathbf{U}_1^T \mathbf{U}_1 \Gamma \mathbf{V}^T \mathbf{V} \Gamma \mathbf{U}_1^T \mathbf{U}_1 \Gamma \left(\frac{1}{2} \right) + \Sigma \left(\frac{1}{2} \right) \mathbf{U}_2^T \mathbf{U}_2 \Sigma \mathbf{V}^T \mathbf{V} \Sigma \mathbf{U}_2^T \mathbf{U}_2 \Sigma \left(\frac{1}{2} \right) \\ &\quad + \Gamma \left(\frac{1}{2} \right) \mathbf{U}_1^T \mathbf{U}_1 \Gamma \mathbf{V}^T \mathbf{V} \Sigma \mathbf{U}_2^T \mathbf{U}_2 \Sigma \left(\frac{1}{2} \right) + \Sigma \left(\frac{1}{2} \right) \mathbf{U}_2^T \mathbf{U}_2 \Sigma \mathbf{V}^T \mathbf{V} \Sigma \mathbf{U}_2^T \mathbf{U}_2 \Sigma \left(\frac{1}{2} \right) \\ &= \Gamma^2 \left(\frac{1}{2} \right) + \Gamma^2 \left(\frac{1}{2} \right) \Gamma^2 + 2 \Sigma \left(\frac{1}{2} \right) \Sigma \Gamma \left(\frac{1}{2} \right) \Gamma + \Sigma^2 \left(\frac{1}{2} \right) \Sigma^2 = 1 + \Gamma. \end{aligned}$$

Now we need to show that columns of $\mathbf{X} \# \mathbf{Y}$ are eigenvectors corresponding to p largest eigenvalues of $\mathbf{X} \mathbf{X}^T + \mathbf{Y} \mathbf{Y}^T$. We note that the eigenvalues of $\mathbf{X} \mathbf{X}^T + \mathbf{Y} \mathbf{Y}^T$ come in pairs of $1 + \Gamma$ and $1 - \Gamma$. This can be readily seen for the case of $p = 1$ as a result of orthogonality of eigenvectors and $\text{Tr}(\mathbf{X} \mathbf{X}^T + \mathbf{Y} \mathbf{Y}^T) = 2p = 2$. The generalization to $p > 1$ follows in the essence similar to Theorem 1 in (Srivastava and Klassen 2004). Since $\Gamma > 0$, then $1 + \Gamma > 1 - \Gamma$, which concludes the proof.

On a related note, one can show that the eigenvalues of $\mathbf{X} \mathbf{X}^T + \mathbf{Y} \mathbf{Y}^T$ are in the form of $1 + \Gamma$ and $1 - \Gamma$ by considering the geodesics between \mathbf{X} and \mathbf{Y} , seen from the mid-point. Without loss of generality, let us assume $\mathbf{X} = \gamma_\# \left(-\frac{1}{2} \right)$ and $\mathbf{Y} = \gamma_\# \left(\frac{1}{2} \right)$, where $\gamma_\#$ is the geodesic written from $\mathbf{M} = \mathbf{X} \# \mathbf{Y}$. This reparametrization is always possible since Grassmann is a quotient space of $\text{SO}(d)$. Now it is easy to show that the eigenvalues of $\gamma_\# \left(\frac{1}{2} \right) \gamma_\#^T \left(\frac{1}{2} \right) + \gamma_\# \left(-\frac{1}{2} \right) \gamma_\#^T \left(-\frac{1}{2} \right)$ are in the form of $1 + \Gamma$ and $1 - \Gamma$. To see this,

$$\begin{aligned} \mathbf{X} &= \mathbf{M} \mathbf{U}_1 \Gamma \left(\frac{-1}{2} \right) - \mathbf{M}_\perp \mathbf{U}_2 \Sigma \left(\frac{-1}{2} \right) \\ &= \mathbf{M} \mathbf{U}_1 \Gamma \left(\frac{1}{2} \right) + \mathbf{M}_\perp \mathbf{U}_2 \Sigma \left(\frac{1}{2} \right). \end{aligned}$$

$$\begin{aligned} \mathbf{Y} &= \mathbf{M}\mathbf{U}_1\Gamma\left(\frac{1}{2}\right) - \mathbf{M}_\perp\mathbf{U}_2\Sigma\left(\frac{1}{2}\right) \\ &= \mathbf{M}\mathbf{U}_1\Gamma\left(\frac{1}{2}\right) - \mathbf{M}_\perp\mathbf{U}_2\Sigma\left(\frac{1}{2}\right). \end{aligned}$$

Now, one can show that

$$\begin{aligned} \mathbf{X}\mathbf{X}^T + \mathbf{Y}\mathbf{Y}^T &= 2\mathbf{M}\mathbf{U}_1\Gamma^2\left(\frac{1}{2}\right)\mathbf{U}_1^T\mathbf{M}^T + 2\mathbf{M}_\perp\mathbf{U}_2\Sigma^2\left(\frac{1}{2}\right)\mathbf{U}_2^T\mathbf{M}_\perp^T \\ &= [\mathbf{M}\mathbf{U}_1 \ \mathbf{M}_\perp\mathbf{U}_2] \begin{bmatrix} 2\Gamma^2\left(\frac{1}{2}\right) & \mathbf{0} \\ \mathbf{0} & 2\Sigma^2\left(\frac{1}{2}\right) \end{bmatrix} [\mathbf{M}\mathbf{U}_1 \ \mathbf{M}_\perp\mathbf{U}_2]^T \\ &= [\mathbf{M}\mathbf{U}_1 \ \mathbf{M}_\perp\mathbf{U}_2] \begin{bmatrix} 1 + \Gamma & \mathbf{0} \\ \mathbf{0} & 1 - \Gamma \end{bmatrix} [\mathbf{M}\mathbf{U}_1 \ \mathbf{M}_\perp\mathbf{U}_2]^T. \end{aligned}$$

Note that the aforementioned proof relies on $d - p \geq p$. If this is not the case, one could simply augment the subspaces by adding sufficient number of zero rows at the bottom of each subspace to facilitate the process. \square

B Tangent-based Computation over Grassmann Manifolds

To compute the logarithm and exponential map over Grassmann manifolds, the orthogonal completion of tall matrices with orthogonal columns needs to be computed. More specifically, for a tall orthogonal matrix like a Grassmann point $\mathbf{X} \in \mathcal{G}(p, d)$, the orthogonal completion \mathbf{Q} is a matrix that satisfies $\mathbf{Q} = [\mathbf{X} | \mathbf{C}]$, $\mathbf{Q}\mathbf{Q}^T = \mathbf{Q}^T\mathbf{Q} = \mathbf{I}_p$.

The orthogonal completion can be computed via Householder reflectors with a complexity of $O(dp^2)$ (Golub and Van Loan 1996). A more efficient algorithm for computing the orthogonal completion is proposed by Gallivan et al. (2003), where the complexity of producing \mathbf{Q} is reduced to $O(p^3)$. The algorithm can be summarized as follows. Let the top and bottom submatrices of \mathbf{X} be respectively denoted by \mathbf{U} and \mathbf{B} , i.e., $\mathbf{X} = \begin{bmatrix} \mathbf{U}_{p \times p} \\ \mathbf{B}_{d-p \times p} \end{bmatrix}$. The orthogonal completion is then:

$$\mathbf{Q}^T = \mathbf{I}_d - \begin{bmatrix} \mathbf{U} - \mathbf{I}_p \\ \mathbf{B} \end{bmatrix} (\mathbf{I}_p - \mathbf{U})^{-1} [(\mathbf{U}^T - \mathbf{I}_p) \ | \ \mathbf{B}]$$

Having \mathbf{Q} , the Grassmann logarithm and exponential maps can be computed as shown in Algorithms 8 and 9, respectively.

Acknowledgements

NICTA is funded by the Australian Government as represented by the *Department of Broadband, Communications and the Digital Economy*, as well as the Australian Research Council through the *ICT Centre of Excellence* program. This work is funded in part through an ARC Discovery grant DP130104567. C. Shen's participation was in part supported by ARC Future Fellowship F120100969.

References

- P.-A. Absil, R. Mahony, and R. Sepulchre. *Optimization Algorithms on Matrix Manifolds*. Princeton University Press, Princeton, NJ, USA, 2008.
- Vincent Arsigny, Pierre Fillard, Xavier Pennec, and Nicholas Ayache. Log-euclidean metrics for fast and simple calculus on diffusion tensors. *Magnetic resonance in medicine*, 56(2): 411–421, 2006.
- E.J. Candes, J. Romberg, and T. Tao. Robust uncertainty principles: exact signal reconstruction from highly incomplete frequency information. *IEEE Transactions on Information Theory*, 52(2):489–509, 2006.

Algorithm 8: Logarithm map over Grassmann manifolds.

Input: The query point \mathbf{X} and point of tangency (pole) \mathbf{P} from the underlying Grassmann manifold $\mathcal{G}(p, d)$, where each point is a subspace in $\mathbb{R}^{d \times p}$.

Output: The logarithm map of \mathbf{X} at tangency point pole \mathbf{P} , *i.e.*, $\log_{\mathbf{P}}(\mathbf{X})$, expressed

$$\text{as } \mathbf{x} = \begin{bmatrix} 0 & \mathbf{A}^T \\ -\mathbf{A} & 0 \end{bmatrix}.$$

Processing.

Compute the $d \times d$ orthogonal completion \mathbf{Q} of \mathbf{P} ;
 Form the $p \times p$ matrix \mathbf{X}_C and $(d-p) \times p$ matrix \mathbf{Y}_C from the top and bottom sub-matrices of $\mathbf{Q}^T \mathbf{X}$, *i.e.*, $\mathbf{Q}^T \mathbf{X} = \begin{bmatrix} \mathbf{X}_C \\ \mathbf{Y}_C \end{bmatrix}$;
 Compute the generalized SVD (Golub and Van Loan 1996) of matrices \mathbf{X}_C and \mathbf{Y}_C to obtain orthogonal matrices $\mathbf{U}_0, \mathbf{U}_1, \mathbf{V}$ and diagonal matrices \mathbf{C} and \mathbf{S} , where $\mathbf{X}_C = \mathbf{U}_0 \mathbf{C} \mathbf{V}^T$, $\mathbf{Y}_C = \mathbf{U}_1 \mathbf{C} \mathbf{V}^T$ and $\mathbf{C}^T \mathbf{C} + \mathbf{S}^T \mathbf{S} = \mathbf{I}_p$;
 Compute the angles θ_i either from the matrix \mathbf{C} or matrix \mathbf{S} , *i.e.*, $\theta_i = \arccos(c_i)$ or $\theta_i = \arcsin(s_i)$, where c_i and s_i are diagonal elements of matrices \mathbf{C} and \mathbf{S} , respectively;
 Form the diagonal matrix $\mathbf{\Theta}$ containing θ_i 's as diagonal elements;
 Compute $\mathbf{A} = \mathbf{U}_0 \mathbf{\Theta} \mathbf{U}_1$;

Algorithm 9: Exponential map over Grassmann manifolds.

Input: The pole \mathbf{P} and a tangent vector $\mathbf{x} \in T_{\mathbf{P}}$ from the underlying Grassmann manifold, where the pole is a subspace in $\mathbb{R}^{d \times p}$.

Output: The exponential map of \mathbf{x} based on the pole \mathbf{P} , *i.e.*, $\exp_{\mathbf{P}}(\mathbf{x})$, computed as

$$\mathbf{Q} \begin{bmatrix} \mathbf{U}_1 \mathbf{\Gamma} \\ -\mathbf{U}_0 \mathbf{\Upsilon} \end{bmatrix}.$$

Processing.

Compute the $d \times d$ orthogonal completion \mathbf{Q} of \mathbf{P} ;
 Form the $(d-p) \times p$ direction matrix \mathbf{A} of \mathbf{x} , where $\mathbf{x} = \begin{bmatrix} 0 & \mathbf{A}^T \\ -\mathbf{A} & 0 \end{bmatrix}$;
 Compute the thin SVD of the direction matrix, *i.e.*, $\mathbf{A} = \mathbf{U}_0 \mathbf{\Theta} \mathbf{U}_1$;
 Compute the diagonal matrices $\mathbf{\Gamma}$ and $\mathbf{\Upsilon}$, where their diagonal elements are $[\mathbf{\Gamma}]_{i,i} = \cos(\theta_i)$ and $[\mathbf{\Upsilon}]_{i,i} = \sin(\theta_i)$. In turn, θ_i 's are the corresponding diagonal elements of $\mathbf{\Theta}$;

- Hasan Ertan Cetingul and René Vidal. Intrinsic mean shift for clustering on stiefel and grassmann manifolds. In *Proc. IEEE Conference on Computer Vision and Pattern Recognition (CVPR)*, pages 1896–1902, 2009.
- Hakan Cevikalp and Bill Triggs. Face recognition based on image sets. In *Proc. IEEE Conference on Computer Vision and Pattern Recognition (CVPR)*, pages 2567–2573, 2010.
- Antoni B. Chan and Nuno Vasconcelos. Probabilistic kernels for the classification of autoregressive visual processes. In *Proc. IEEE Conference on Computer Vision and Pattern Recognition (CVPR)*, pages 846–851, 2005. ISBN 0-7695-2372-2.
- Shaokang Chen, Conrad Sanderson, Mehrtash Harandi, and Brian C. Lovell. Improved image set classification via joint sparse approximated nearest subspaces. In *Proc. IEEE Conference on Computer Vision and Pattern Recognition (CVPR)*, pages 452–459, 2013.
- Yasuko Chikuse. *Statistics on Special Manifolds*, volume 174. Springer, 2003.
- Katrien De Cock and Bart De Moor. Subspace angles between ARMA models. *Systems and Control Letters*, 46:265–270, 2002.
- D. Comaniciu and P. Meer. Mean shift: A robust approach toward feature space analysis. *IEEE Trans. Pattern Analysis and Machine Intelligence*, 24(5):603–619, 2002.

- Navneet Dalal and Bill Triggs. Histograms of oriented gradients for human detection. In *Proc. IEEE Conference on Computer Vision and Pattern Recognition (CVPR)*, pages 886–893, 2005.
- Gianfranco Doretto, Alessandro Chiuso, Ying Nian Wu, and Stefano Soatto. Dynamic textures. *Int. Journal of Computer Vision*, 51:91–109, 2003.
- Michael Elad. *Sparse and Redundant Representations - From Theory to Applications in Signal and Image Processing*. Springer, 2010.
- Masoud Faraki, Mehrtash T. Harandi, Arnold Wiliem, and Brian C. Lovell. Fisher tensors for classifying human epithelial cells. *Pattern Recognition*, 2013.
- K.A. Gallivan, A. Srivastava, Xiuwen Liu, and P. Van Dooren. Efficient algorithms for inferences on Grassmann manifolds. In *IEEE Workshop on Statistical Signal Processing*, pages 315–318, 2003.
- Bernard Ghanem and Narendra Ahuja. Maximum margin distance learning for dynamic texture recognition. In *Proc. European Conference on Computer Vision (ECCV)*, volume 6312, pages 223–236, 2010.
- Gene H. Golub and Charles F. Van Loan. *Matrix computations (3rd ed.)*. Johns Hopkins University Press, Baltimore, MD, USA, 1996. ISBN 0-8018-5414-8.
- Boqing Gong, Yuan Shi, Fei Sha, and Kristen Grauman. Geodesic flow kernel for unsupervised domain adaptation. In *Proc. IEEE Conference on Computer Vision and Pattern Recognition (CVPR)*, pages 2066–2073, 2012.
- R. Gopalan, R. Li, and R. Chellappa. Unsupervised adaptation across domain shifts by generating intermediate data representations. *IEEE Trans. Pattern Analysis and Machine Intelligence*, 2013.
- Michael Grant and Stephen Boyd. Graph implementations for nonsmooth convex programs. In *Recent Advances in Learning and Control*, Lecture Notes in Control and Information Sciences, pages 95–110. Springer-Verlag Limited, 2008.
- Michael Grant and Stephen Boyd. CVX: Matlab software for disciplined convex programming, version 2.0 beta. <http://cvxr.com/cvx>, September 2012.
- Jihun Hamm and Daniel D. Lee. Grassmann discriminant analysis: a unifying view on subspace-based learning. In *Proc. Int. Conference on Machine Learning (ICML)*, pages 376–383, 2008.
- Mehrtash Harandi, Conrad Sanderson, Chunhua Shen, and Brian C. Lovell. Dictionary learning and sparse coding on grassmann manifolds: An extrinsic solution. In *Proc. Int. Conference on Computer Vision (ICCV)*, December 2013a.
- Mehrtash T. Harandi, Conrad Sanderson, Sareh Shirazi, and Brian C. Lovell. Graph embedding discriminant analysis on Grassmannian manifolds for improved image set matching. In *Proc. IEEE Conference on Computer Vision and Pattern Recognition (CVPR)*, pages 2705–2712, 2011.
- Mehrtash T. Harandi, Conrad Sanderson, Richard Hartley, and Brian C. Lovell. Sparse coding and dictionary learning for symmetric positive definite matrices: A kernel approach. In *Proc. European Conference on Computer Vision (ECCV)*, pages 216–229, 2012.
- Mehrtash T. Harandi, Conrad Sanderson, Sareh Shirazi, and Brian C. Lovell. Kernel analysis on Grassmann manifolds for action recognition. *Pattern Recognition Letters*, 34(15):1906 – 1915, 2013b.
- Richard Hartley, Jochen Trumpf, Yuchao Dai, and Hongdong Li. Rotation averaging. *Int. Journal of Computer Vision*, 103(3):267–305, 2013.
- Uwe Helmke, Knut Hüper, and Jochen Trumpf. Newtons method on Grassmann manifolds. *Preprint: arXiv:0709.2205*, 2007.
- Jeffrey Ho, Yuchen Xie, and Baba Vemuri. On a nonlinear generalization of sparse coding and dictionary learning. In *Proc. Int. Conference on Machine Learning (ICML)*, pages 1480–1488, 2013.
- Roger A Horn and Charles R Johnson. *Matrix analysis*. Cambridge University Press, 2012.
- Sadeep Jayasumana, Richard Hartley, Mathieu Salzmann, Hongdong Li, and Mehrtash Harandi. Kernel methods on the Riemannian manifold of symmetric positive definite matrices. In *Proc. IEEE Conference on Computer Vision and Pattern Recognition (CVPR)*, 2013.
- Minyoung Kim, Sanjiv Kumar, Vladimir Pavlovic, and Henry Rowley. Face tracking and recognition with visual constraints in real-world videos. In *Proc. IEEE Conference on Computer Vision and Pattern Recognition (CVPR)*, pages 1–8, 2008.
- Tae-Kyun Kim and Roberto Cipolla. Canonical correlation analysis of video volume tensors for action categorization and detection. *IEEE Trans. Pattern Analysis and Machine Intel-*

- ligence*, 31(8):1415–1428, 2009.
- Tae-Kyun Kim, J. Kittler, and R. Cipolla. Discriminative learning and recognition of image set classes using canonical correlations. *IEEE Trans. Pattern Analysis and Machine Intelligence*, 29(6):1005–1018, 2007.
- John M Lee. *Introduction to smooth manifolds*, volume 218. Springer, 2012.
- Binlong Li, M. Ayazoglu, T. Mao, O.I. Camps, and M. Szaier. Activity recognition using dynamic subspace angles. In *Proc. IEEE Conference on Computer Vision and Pattern Recognition (CVPR)*, pages 3193–3200, 2011.
- Yui Man Lui. Human gesture recognition on product manifolds. *Journal of Machine Learning Research*, 13:3297–3321, 2012.
- Julien Mairal, Francis Bach, and Jean Ponce. Task-driven dictionary learning. *IEEE Trans. Pattern Analysis and Machine Intelligence*, 34(4):791–804, 2012.
- Timo Ojala, Matti Pietikäinen, and Topi Mäenpää. Multiresolution gray-scale and rotation invariant texture classification with local binary patterns. *IEEE Trans. Pattern Analysis and Machine Intelligence*, 24:971–987, July 2002.
- Bruno A. Olshausen and David J. Field. Emergence of simple-cell receptive field properties by learning a sparse code for natural images. *Nature*, 381(6583):607–609, 1996.
- Sam T Roweis and Lawrence K Saul. Nonlinear dimensionality reduction by locally linear embedding. *Science*, 290(5500):2323–2326, 2000.
- Conrad Sanderson, Mehrtash T. Harandi, Yongkang Wong, and Brian C. Lovell. Combined learning of salient local descriptors and distance metrics for image set face verification. In *Proc. Int. Conf. Advanced Video and Signal-Based Surveillance*, pages 294–299, 2012.
- Aswin Sankaranarayanan, Pavan Turaga, Richard Baraniuk, and Rama Chellappa. Compressive acquisition of dynamic scenes. In *Proc. European Conference on Computer Vision (ECCV)*, volume 6311, pages 129–142, 2010.
- John Shawe-Taylor and Nello Cristianini. *Kernel Methods for Pattern Analysis*. Cambridge University Press, 2004.
- Anuj Srivastava and Eric Klassen. Bayesian and geometric subspace tracking. *Advances in Applied Probability*, 36(1):43–56, 2004.
- Raghav Subbarao and Peter Meer. Nonlinear mean shift over Riemannian manifolds. *Int. Journal of Computer Vision*, 84(1):1–20, 2009.
- P. Turaga, A. Veeraraghavan, A. Srivastava, and R. Chellappa. Statistical computations on Grassmann and Stiefel manifolds for image and video-based recognition. *IEEE Trans. Pattern Analysis and Machine Intelligence*, 33(11):2273–2286, 2011.
- Matthew Turk and Alex Pentland. Eigenfaces for recognition. *Journal of Cognitive Neuroscience*, 3(1):71–86, 1991.
- Oncel Tuzel, Fatih Porikli, and Peter Meer. Pedestrian detection via classification on Riemannian manifolds. *IEEE Trans. Pattern Analysis and Machine Intelligence*, 30:1713–1727, October 2008.
- Raviteja Vemulapalli, Jaishanker K Pillai, and Rama Chellappa. Kernel learning for extrinsic classification of manifold features. In *Proc. IEEE Conference on Computer Vision and Pattern Recognition (CVPR)*, pages 1782–1789, 2013.
- Paul Viola and Michael J Jones. Robust real-time face detection. *Int. Journal of Computer Vision*, 57(2):137–154, 2004.
- Jinjun Wang, Jianchao Yang, Kai Yu, Fengjun Lv, Thomas Huang, and Yihong Gong. Locality-constrained linear coding for image classification. In *Proc. IEEE Conference on Computer Vision and Pattern Recognition (CVPR)*, pages 3360–3367, 2010.
- Yang Wang and Greg Mori. Human action recognition by semilattent topic models. *IEEE Trans. Pattern Analysis and Machine Intelligence*, 31(10):1762–1774, 2009.
- J. Wright, A.Y. Yang, A. Ganesh, S.S. Sastry, and Y. Ma. Robust face recognition via sparse representation. *IEEE Trans. Pattern Analysis and Machine Intelligence*, 31(2):210–227, 2009.
- Yong Xu, Yuhui Quan, Haibin Ling, and Hui Ji. Dynamic texture classification using dynamic fractal analysis. In *Proc. Int. Conference on Computer Vision (ICCV)*, 2011.
- Jianchao Yang, Kai Yu, Yihong Gong, and T. Huang. Linear spatial pyramid matching using sparse coding for image classification. In *Proc. IEEE Conference on Computer Vision and Pattern Recognition (CVPR)*, pages 1794–1801, 2009. ISBN 978-1-4244-3992-8.
- Kai Yu, Tong Zhang, and Yihong Gong. Nonlinear learning using local coordinate coding. In *Proc. Advances in Neural Information Processing Systems (NIPS)*, pages 2223–2231, 2009a.

-
- S. Yu, T. Tan, K. Huang, K. Jia, and X. Wu. A study on gait-based gender classification. *IEEE Trans. Image Processing (TIP)*, 18(8):1905–1910, 2009b.
- Guoying Zhao and Matti Pietikainen. Dynamic texture recognition using local binary patterns with an application to facial expressions. *IEEE Trans. Pattern Analysis and Machine Intelligence*, 29(6):915–928, 2007.
- S. Zheng, J. Zhang, K. Huang, R. He, and T. Tan. Robust view transformation model for gait recognition. In *International Conference on Image Processing (ICIP)*, pages 2073–2076, 2011.